Agenzia Nazionale per le Nuove Tecnologie,
l'Energia e lo Sviluppo Economico Sostenibile

Ministero dello Sviluppo Economico

RICERCA DI SISTEMA ELETTRICO

CERSE-POLIMI RL 1134/2010

Prove sperimentali per canali in paralleli e relative zone di instabilità

D. Papini, M.E. Ricotti

Report RdS/2010/83

PROVE SPERIMENTALI PER CANALI IN PARALLELI E RELATIVE ZONE DI INSTABILITÀ

D. Papini, M.E. Ricotti

Settembre 2010

Report Ricerca di Sistema Elettrico
Accordo di Programma Ministero dello Sviluppo Economico – ENEA
Area: Produzione e fonti energetiche
Tema: Nuovo Nucleare da Fissione

Responsabile Tema: Stefano Monti, ENEA

CIRTEN

CONSORZIO INTERUNIVERSITARIO

PER LA RICERCA TECNOLOGICA NUCLEARE

POLITECNICO DI MILANO

DIPARTIMENTO DI ENERGIA, Sezione INGEGNERIA NUCLEARE-CeSNEF

Prove sperimentali per canali in parallelo e relative zone di instabilità

Davide Papini, Marco Colombo, Antonio Cammi, Marco Ricotti

CERSE-POLIMI RL-1134/2010

Milano, Agosto 2010

Lavoro svolto in esecuzione della linea progettuale LP2– punto G.1

INDEX

EXECUTIVE SUMMARY

This document describes the research activities carried out by Politecnico di Milano on the field of two-phase flow instabilities in parallel channels.

Density Wave Oscillations (DWOs) are probably the most common type of instabilities affecting vapour generation in boiling systems. They are "dynamic type" instabilities, which result from multiple feedback effects between the flow rate, the vapour generation rate and the pressure drops in the boiling channel. These instabilities constitute an issue of special interest both for Boiling Water Reactor (BWR) fuel channels (where they are moreover coupled through the neutronic feedback with the neutron field), and for parallel tubes of innovative steam generators. Extensive attention is required because parallel channel instability is very difficult to be immediately detected when occurs in steam power systems (widely used in the nuclear area). The total mass flow of the system remains in fact stable while the instability is locally triggered among some of the parallel channels. Thermally induced oscillations of the flow rate and system pressure are undesirable, as they can cause mechanical vibrations, problems of system control, and in extreme circumstances disturb the heat transfer characteristics so that the heat transfer surface may burn-out. Large amplitude fluctuations in the heater wall temperature (so named "thermal oscillations") usually occur under DWO conditions. Continual cycling of the wall temperature can lead to thermal fatigue problems which may cause tube failure.

It is clear from these examples that the flow instabilities must be avoided, especially in the design of nuclear systems. The safe operating regime of a two-phase heat exchanger can be determined by the instability threshold values of such system parameters as flow rate, pressure, inlet temperature and exit quality. To the aim, both basic experiments and numerical analyses are necessary.

Density wave oscillations in parallel channels, with reference to steam generator tubes case, represent hence the topic of the present study. The modelling effort currently underway at the Nuclear Engineering Division of the Department of Energy (Politecnico di Milano) – dealing with two helically coiled tubes of the IRIS (International Reactor Innovative and Secure) steam generator – is described. DWO instability threshold and the influence of the different thermal-hydraulic parameters (thermal power, flow rate, pressure, channel inlet throttling and subcooling) are being studied via an analytical dynamic model based on the integration of 1D governing equations and via the well known "six-equations" system code RELAP5. The adoption of simple homogeneous equilibrium models is well established to study basic thermal-hydraulic phenomena; on the contrary, the use of complex numerical system codes represents a reliable option, since they can provide accurate quantitative predictions with simple and straightforward nodalizations.

The main objective of these analyses has been to prepare an experimental campaign at SIET labs (Piacenza), where such instability phenomenon is being directly investigated with a test section reproducing in full scale two helical tubes of the IRIS steam generator. The whole campaign is expected to provide a unique evidence of the influence of the helical shape (through the centrifugal field induced by tube bending) on instability occurrence, as well as a useful experimental database for model validation.

Preparation of the experimental campaign, with description of the used test section and proposed experimental procedure and test matrix, is discussed in Section 1 of the document. Section 2 is dedicated to the RELAP5 modelling of

boiling channel instability, mainly devoted to a methodological assessment of the capability of the code to detect the onset on instability (a single boiling channel, with proper definition of the exact boundary conditions, is mainly referenced, rather than the two long parallel channels object of the experimental campaign). Pre-test analysis, carried out with an analytical dynamic model developed ad hoc for theoretical prediction of the instability threshold, is discussed in Section 3. Finally, the first experimental results on DWO inception (July 2010) are presented in Section 4. Preliminary argumentations about the triggering event of the instability and interpretation of the period of oscillations are proposed.

1 PREPARATION OF THE EXPERIMENTAL CAMPAIGN

1.1 Introductory background on boiling channel instabilities

Two-phase flow instabilities have been widely studied in the past because they are of interest to the design and operation of many industrial systems, such as boiling water reactors or steam generators. The various types of self-sustained oscillations which could arise in a boiling channel have been reviewed and classified in different literature works [1][2]. Amongst them, density wave oscillations in parallel channels – with respect to steam generator parallel tubes – represent the object of the developed experimental campaign.

The origin of this instability is ascribed to the difference in density between the fluid entering the heated channel (subcooled liquid) and the fluid exiting (low density two-phase mixture), which triggers delays in the transient distribution of pressure drops along the duct and may lead to self-sustained oscillations. A constant-pressure-drop (or better, the same, not necessarily constant with time, pressure drop for the two channels) is the proper boundary condition which can excite those dynamic feedbacks which are at the source of the instability mechanism.

The physical mechanism leading to density wave oscillations is investigated since the '60, and, for the sake of clarity, is briefly summarized in the followings [3].

A single heated channel is considered for simplicity. The instantaneous position of the boiling boundary, that is the point where the bulk of the fluid reaches saturation, divides the channel into a single-phase region and a two-phase region. A sudden outlet pressure drop perturbation, e.g. resulting from a local microscopic increase in void fraction, can be assumed to trigger the instability by propagating a corresponding low pressure pulse to the channel inlet, which in turn causes an increase in inlet flow. Considered as a consequence an oscillatory inlet flow entering the channel [4], a propagating enthalpy perturbation is created in the single-phase region. The boiling boundary will respond by oscillating according to the amplitude and the phase of the enthalpy perturbation at the point where the flow reaches saturation. Changes in the flow and in the length of the single-phase region will combine to create an oscillatory, single-phase, pressure drop perturbation (named $\delta\Delta P_1$). The enthalpy perturbation will appear in the two-phase region as quality and void fraction perturbations and will travel with the flow along the channel (heavier fluid wave propagation). The combined effects of flow and void fraction perturbations and the variation of the two-phase length will create a two-phase pressure drop perturbation (named $\delta\Delta P_2$). Since the total pressure drop across the boiling channel is imposed ($\delta\Delta P_{tot} = \delta\Delta P_1 + \delta\Delta P_2 = 0$), the two-phase pressure drop perturbation will create a feedback pressure perturbation of the opposite sign in the single-phase region (lighter fluid wave propagation), which may attenuate or reinforce the initial imposed perturbation. With correct timing, the flow oscillation can become self-sustained, matched by an oscillation of pressure and by the single-phase and two-phase pressure drop terms oscillating in counter-phase.

The period of the oscillations is closely related to transportation delays in the channel. In the single-phase region enthalpy perturbations propagate with the flow velocity [3]. In the two-phase region void fraction disturbances created by the enthalpy perturbations, according to Zuber and Staub [5][6], propagate with kinematic-wave velocity, which is of the order of magnitude of the velocity of the vapour phase. Since a complete oscillating cycle consists in the passage of two perturbations through the channel (positive "heavier fluid" wave and negative "lighter fluid" wave), the period of the oscillations should be in the range of twice the mixture transit time in the heated section:

$$T = 2\tau \tag{1}$$

On the other hand, the classical interpretation of density wave oscillations still confirmed by the noteworthy review of Kakaç and Bon [2] on two-phase flow dynamic instabilities, sounds well recognized and accepted just under low inlet subcooling conditions. At high inlet subcooling, instead, a different description has been raised by Ambrosini et al. [7], on the basis of the criticism on classical point of view due to Podowski [8] and Rizwan-Uddin [9]. Their explanation is based on the different speeds of propagation of velocity perturbations between the single-phase region (speed of sound) and the two-phase region (kinematic velocity). Briefly, at high inlet subcooling DWO phenomenon looks mostly governed by flow perturbations rather than by actual density wave perturbations, and the period of the oscillations may be considerably longer than twice the fluid transit time.

1.2 Stability maps – parametric effects

For stability investigations, the task of the analyst is to find the regions of stable and unstable operation in the three-dimensional space given by the channel flow rate w, thermal power q and inlet subcooling Δh_{in} (in enthalpy units). A mapping of these regions in two dimensions is referred to as the stability map of the system (at a given pressure level).
No universal map exists. Furthermore, the stability boundary in the (w, q, Δh_{in}) space is a surface and can be represented only by a family of curves in any two-dimensional map. Hence, the usage of dimensionless stability maps is strongly recommended to cluster the information on the dynamic characteristics of the system.
The most used dimensionless stability map is due to Ishii and Zuber [10], and it consists of a phase change number N_{pch} versus a subcooling number N_{sub}.
The phase change number is the ratio of the characteristic frequency of phase change Ω to the inverse of a single-phase transit time in the system:

$$N_{pch} = \frac{\Omega}{\frac{V_{in}}{L}} = \frac{\frac{q}{AL}\frac{v_{fg}}{h_{fg}}}{\frac{V_{in}}{L}}$$

$$w = \rho_f V_{in} A$$

$$N_{pch} = \frac{q}{w h_{fg}} \frac{v_{fg}}{v_f} \tag{2}$$

The subcooling number reads:

$$N_{sub} = \frac{\Delta h_{in}}{h_{fg}} \frac{v_{fg}}{v_f} \tag{3}$$

Figure 1 shows a typical stability map for a two parallel channel system, as obtained by the theoretical study of Guo Yun et al. [11] (see also the work of Zhang et al. [12]).
The typical stability boundary shape is usually a classical inclination "L" at some operating conditions (that is, when the system pressure is reasonably low and the inlet resistance coefficient is small). The stability boundary at high inlet subcooling, on the space of $N_{pch} - N_{sub}$, is a line of constant equilibrium quality. In Figure 1, the results of preliminary calculations with the RELAP5 code for the same two channels configuration are reported as well. Such results have to be intended just as a qualitative specimen of what can be the goal of a stability investigation on density wave

oscillations. The theoretical results of Guo Yun et al. [11] (Figure 1-a), based on a homogeneous flow model, may be conservative in terms of predicting the stability boundary. The numerical results obtained with RELAP5 (Figure 1-b) may be affected by thermal crisis occurrence within the channels, as well as by numerical diffusion.

In the following parametric discussion, the influence of a change in a certain parameter is said to be stabilizing if it tends to take the operating point from the unstable to the stable region.

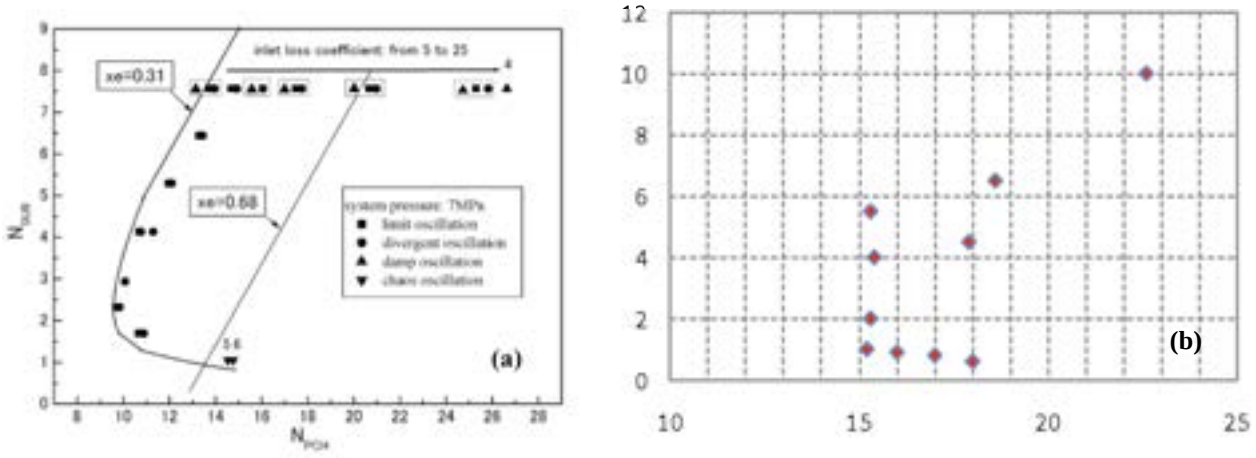

Figure 1 - Stability map on the space N_{pch}-N_{sub} for a two parallel channel system: theoretical results of Guo Yun et al. [11] (a) and RELAP5 simulations (b).

1.2.1 Effects of heat input, flow rate and exit quality

A stable system is brought into the unstable operating region by increases in heat input or decreases in flow rate; both effects increase the exit quality, hence the vapour compressibility effects which trigger flow oscillations.

The destabilizing effect of increasing the ratio *q/w* seems to be universally accepted, although islands of instability have been observed to occur by Yadigaroglu and Bergles [13] within the stable operating region (higher-mode oscillations obtained by reducing slowly and continuously the inlet flow rate).

1.2.2 Effects of pressure level

An increase of pressure level has always been found to be stabilizing, although one must be careful in stating which system parameters were kept constant while the pressure level was increased. At constant values of the dimensionless subcooling and exit quality, the pressure effect is made apparent by the density ratio v_{fg}/v_f (approximately equal to ρ_f/ρ_g). However, it is worth to point out that pressure influence is the less effective on the stability boundary, as confirmed for instance by Van Bragt and Van Der Hagen [14]. Moreover, Ishii [15] noted that calculated stability boundaries at three different pressure levels could not be differentiated in the (N_{pch}, N_{sub}) space.

1.2.3 Effects of inlet subcooling

The influence of inlet subcooling on the system stability is multi-valued. In the high inlet subcooling region the stability is strengthened by increasing the subcooling, whereas in the low inlet subcooling region the stability is strengthened by

decreasing the subcooling. That is, the inlet subcooling is stabilizing at high subcoolings and destabilizing at low subcoolings.

Intuitively this effect may be explained by the fact that, as the inlet subcooling is increased or decreased, the two-phase channel tends towards stable single-phase liquid and vapour operation, respectively. Thus, according to which stable region is closer, increases and decreases of subcooling tend to pull the system out of the unstable two-phase operating mode.

1.2.4 Effects of inlet and exit throttling

The effect of inlet throttling (single-phase region pressure drops) is always strongly stabilizing and is used to assure the stability of otherwise unstable channels.

On the contrary, the effect of flow resistances near the exit of the channel (two-phase region pressure drops) is strongly destabilizing. For example, stable channels can become unstable if an orifice is added at the exit, or if a riser section is provided.

1.3 Starting point experimental data

The most valuable experimental work available in open literature for the set-up of the campaign on parallel channel instabilities is due to Masini et al. [16]. A forced convection open loop circuit (IETI-1 facility) is built to obtain more than 200 flow instability threshold data. The circuit is composed of two parallel straight channels.

The mentioned paper is a lesson as the experimental procedure and flow instability detection method are concerned (The step-by-step description is given in Section 1.5 with reference to the presented facility with parallel helical heated tubes).

The experimental apparatus comprehends a throttling valve after tube preheater, which introduces a strong localized pressure drop on the feeding line (ΔP_b = 30 bar).

Each channel is provided with two valves at inlet (V_0 and V_I) and one valve at outlet (V_v). V_0 simulates the reactor flow distribution orifice. The pressure drop across V_I is utilized as flow rate signal. V_v is introduced to study the effect of a pressure loss at channel outlet. In all the experiments these three sets of valves are manually adjusted in two different positions, either fully open (f.o.) or partially closed (p.c.).

A riser section is provided for each channel (destabilizing effect for instability threshold), before the common outlet discharge.

Parallel channel flow instability is studied for the following values of parameters:

- three levels of pressure (P): 50 – 30 – 10 bar;
- two levels of mass flow rate (w): 266 – 133 kg/h;
- different configurations concerning the valve positions;
- inlet subcooling from -20% ÷ -30% to ~0 for each set of P, w and valve positions.

For the sake of brevity, threshold data with just a particular configuration of valves are presented in this document. V_I (at inlet) and V_v (at outlet) are p.c.; V_0 (at inlet) is f.o.. It is worth noticing that the Authors deal with concentrated pressure drops at valves in terms of ΔP, and not in terms of the respective form loss coefficients k. That is, when the

two different values of flow rate are experienced (w_1 = 133 kg/h – w_2 = 266 kg/h), V_Γ and V_v throttling is adjusted in order to respect always:

- ΔP_Γ = 10 kPa;
- ΔP_v = 20 kPa (characterization of the valve done with a liquid fluid flowing, i.e. cold water at 20 °C and double flow rate value).

Parallel channel flow instability thresholds can be presented in a dimensional form, plotting the limit power (at oscillations inception) as a function of inlet subcooling, at different flow rates and pressures (Figure 2-a). It is apparent that threshold power *q* increases with increasing *w* and *P*. Reasoning in terms of power-over-flow ratio (*q/w*), the curves at different flow rate but equal pressure are quite overlapped (Figure 2-b), confirming the statement of Par. 1.2.1. The most influencing parameter for density wave oscillations appearance is thus *q/w*, being strictly linked to the exit quality which triggers the whole phenomenon.

Limit power dependence on inlet subcooling is instead complex, but it is enough to confirm the conclusions drawn in Par 1.2.3: increasing the inlet subcooling is stabilizing for high subcooling values, and destabilizing for low subcooling values.

Moreover, the importance of the ratio *q/w* as regards the instability inception is at the basis of the usage of non-dimensional maps for stability investigations. Working on the N_{pch} - N_{sub} space, for instance, permits to establish a stability boundary which is independent on the actual flow rate experienced. This concern is clearly shown in Figure 3, where stability thresholds at the three different pressure values are reported. Stability boundary behaviour at different pressures, finally, is not easily understandable with this kind of map, where the two dimensionless groups should be built such to be insensitive on the pressure level. The stabilizing effect of an increasing pressure is evident considering the constant equilibrium quality line in the upper portion of the boundary: limit power increases with pressure, and limit equilibrium quality increases as well.

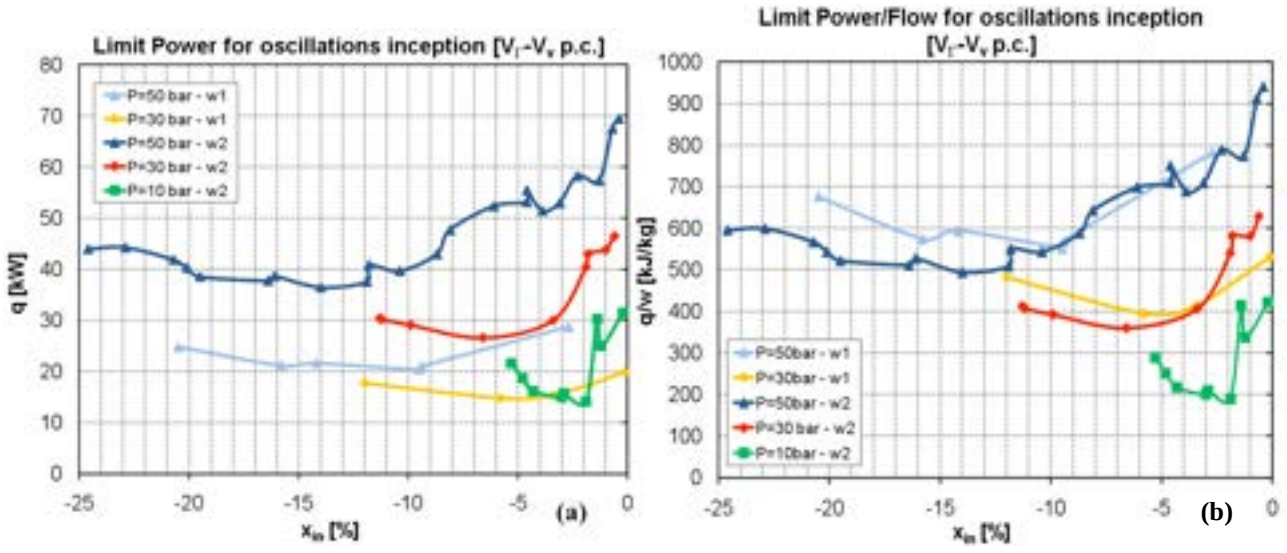

Figure 2 - Influence of flow rate, pressure and inlet subcooling on threshold power.
With throttling at inlet (V_Γ) and outlet (V_v), according to what it is defined in the text.

Various valve positions are investigated in the Article. Most significant results are given in Figure 4 (considered the highest level of pressure and mass flow). With respect to the "fully open valves" configuration (blue points), both the stabilizing effect of an inlet concentrated pressure drop and the destabilizing effect of an outlet concentrated pressure drop can be observed. The cases with a throttling both at inlet and outlet (gold and red points) are more unstable rather than the basic case (blue points), because of the stronger effect of a form loss at outlet than at inlet.

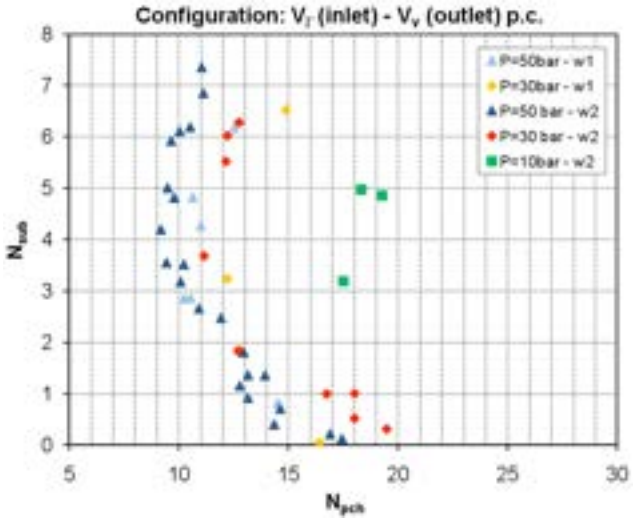

Figure 3 - Stability maps at different flow conditions [case with V_Γ-V_v p.c.].

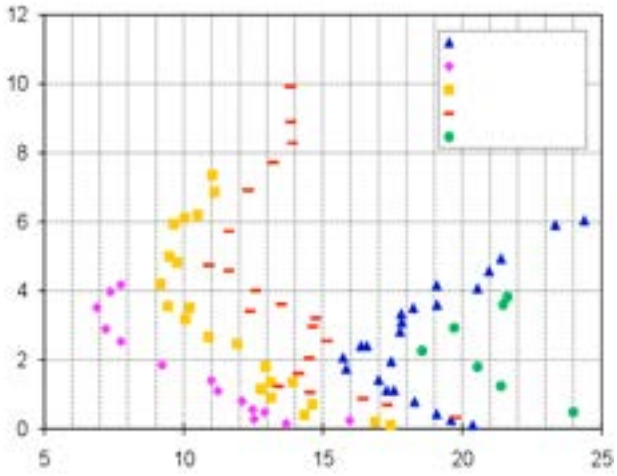

Figure 4 - Stability maps at different valve position configurations [case with P = 50 bar – w = 266 kg/h].
VG → valve at inlet; Vv → valve at outlet

1.4 The experimental facility

Investigated experimental facility was built and operated at SIET labs in Piacenza, as an extension of an electrically heated test section used for the investigation of the thermal-hydraulics (two-phase pressure drops – under diabatic and adiabatic conditions – and dryout thermal crisis occurrence) in a helical-coil steam generator tube [17], already expanded to simulate a passive emergency heat removal system with natural circulation [18].

Original test section framed in the facility represents one single helical tube of IRIS SG. Coil diameter (1 m) has been chosen as representative of a mean value of IRIS SG tube, while tube inner diameter (12.53 mm) is the commercially scheduled value nearer to IRIS real value (13.24 mm). The heated tube is thermally insulated by means of rock wool. The thermal losses were already measured via runs with single-phase hot pressurized water flowing inside the steam generator, and estimated as a function of the temperature difference between external tube wall and the environment.

Renewed design of the facility for flow instability detection comprised the adding of a second helical tube identical to the first one (same coil diameter, pitch and length), its instrumentation and its insulation with rock wool. The two helices have been connected with common lower and upper header to provide the equal-pressure-drop boundary condition required for the instability inception. The conceptual sketch of the new facility with the two electrically heated parallel helically coiled tubes is depicted in Figure 5.

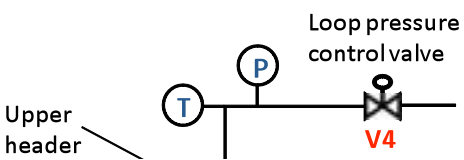

The whole facility is made by a supply section and a test section.

The supply section feeds demineralized water from a tank to the test section, by means of a centrifugal booster pump and a feed-water pump, i.e. a volumetric three-cylindrical pump with a maximum head of about 200 bar driven by an asynchronous three-phases motor. Water is demineralised via an ionic exchanger resin bed, thus obtaining an electrical conductivity value for the fluid of about 1.5 μS/cm. The flow rate is controlled by a throttling valve (V3) positioned downwards the feed water pump and after a bypass line. System pressure control is accomplished by acting on a throttling valve (V4) placed at the end of the steam generator, whose degree of throttle is manually imposed by acting on a pneumatic actuator until the desired pressure is reached.

An electrically heated helically coiled pre-heater is located before the test section, and allows creating the desired temperature at the inlet of the test section. The test section in Figure 5 is electrically heated via Joule effect by DC current. Two distinct, independently controllable and contiguous sections are provided: the first one simulates the subcooling zone and the two-phase zone of the steam generator, while the second one was used in the past [17] to simulate the post dryout and superheating zone.

The possibility of controlling thermal flux in the two zones could allow to roughly simulate the variation in heat flux that occurs in a real once-through steam generator.

Table 1 - Test section main data.

Tube material	SS AISI 316L
Inner diameter, d [mm]	12.53
Outer diameter [mm]	17.24
Coil diameter, D [mm]	1000
Coil pitch [mm]	800
Tube length [m]	32
Steam generator height [m]	8

The main data of the two steam generator coiled tubes are listed in Table 1.

An accurate measurement of the total flow rate is obtained by a Coriolis flow-meter, placed between the pump and the pre-heater. The maximum error is about 0.3%, in the range of the explored flow rates.

The bulk temperatures are measured with a K-class thermocouple drowned in a small well at steam generator inlet and outlet headers. All the measurement devices have been tested and calibrated at the certified SIET labs (SIT certified).

The water pressures at inlet and outlet headers are measured by absolute pressure transducers (maximum error of about 0.1%); nine pressure taps are disposed nearly every 4 m along one coiled tube and eight differential pressure transducers (maximum error of about 0.4%) connect the pressure taps.

Electric power is supplied to the steam generator via Joule effect using low voltage (a hundred Volts)-high amperage current. The electric power generator is the coupling of a AC transformer (from 130 kV to 3 kV) with a Chopper that converts alternate current into (nearly) direct current. Electrical power was obtained via separate measurement of current (by a shunt) and voltage drop along the test section by a voltmeter. The uncertainty in steam generator power balances was estimated to be 2.5%.

Just some comments are remarked in the followings, in order to clarify most crucial points for the preparation and execution of the experimental campaign on parallel channel instability.

- Test section electrical heating is considered in the current configuration, that is via Joule effect by DC current just on the first section of the two helical tubes (length of 24 m). Hence, a riser unheated section (length of 8 m) is considered. Moving the electrical terminals on the tubes could permit to investigate the influence of riser sections (though this is not a priority for the experimental campaign).
- Each tube is provided at inlet with a calibrated orifice (with a differential pressure transmitter) used to measure the flow rate in each channel and to visually detect the instability inception, and with a valve to impose a concentrated pressure drop (stabilizing on the system behaviour). V1 and V2 represent the total stabilizing pressure drops (instrumented orifice + valve) introduced at the inlet of the two helical tubes respectively.
- Wall thermocouples are mounted on the two coils to identify the risk of dryout crisis occurrence.
  As a matter of fact, it is known [16] that thermal crisis can be reached by increasing the supplied power to get the instability threshold. More in detail, the two values of power *q* corresponding to flow oscillation threshold and to heat transfer crisis are nearly undistinguishable at high inlet subcooling; the difference increases for low inlet subcooling.

1.5 Proposed experimental procedure

In order to excite flow unstable conditions starting from stable operating conditions, it has been proposed to gradually increase (by small steps) the electrical power supplied to the heated elements from nominal values up to the appearance of flow instability.

Flow instability power threshold can be experimentally defined as that power corresponding to the smallest permanent and regular flow oscillation, detected by visual observation of the pressure drop recording of the calibrated orifices (within V1 and V2 of Figure 5). An extrapolation toward zero of the oscillation amplitude plotted against the power input can also be used to define the threshold power level.

The approaching to instability inception by small increases of supplied power is preferred rather than changing (reducing) the mass flow rate, since a change in flow rate affects the amount of pressure drops concentrated at the valves before the heated tubes, and because of the strange instability behaviour observed by Yadigaroglu and Bergles [13]. On the other hand, approaching the instability by changing the inlet subcooling (via preheater power) is thoughtless due to the complicated effect that this parameter has on system stability.

The proposed test procedure can be summarized in the following steps:

(1) Registration of the gravitational head of the different instruments.
(2) Characterization of the normal behaviour of the system (for instance, check that, at open V1 and V2 valves, the flow rate is reasonably balanced between the two coils).
(3) Impose a defined position of V1 and V2 valves.
(4) Define a pressure level (start from higher pressure toward lower pressure).
(5) Impose a value of flow rate.
(6) Impose a value of inlet subcooling by means of the preheater.

(7) Reach the desired pressure level by generating vapour with a power increase. When the desired pressure is obtained, keep the system in a steady-state condition (measurements of temperature, pressure, flow rate and heat input).

(8) The electrical power is progressively increased by a small amount (small steps of 2-5 kW per tube), until sustained oscillations are observed (check that the system pressure remains more or less constant).

(9) Once the instability is recorded, bring the system back to step 6, and change the subcooling. Repeat step 7 up to the instability (same operating pressure).

(10) Once all the subcooling values are tested for a flow rate level, change the flow rate and repeat steps 6, 7 and 8.

(11) Once all the flow rate values defined in step 5 are completely explored (every subcooling value), change the desired pressure level (at least x3) and repeat steps 5 – 9.

(12) Finally, change the valve position (step 3) and repeat the whole procedure (steps 4 – 11).

The proposed procedure is based on a minimization of the actions required on the circuit valves, at the cost of many changes in the pressure level during the tests execution. If this issue is considered more critical, it can be thought to experience the various valve configurations (changing automatically from control room the throttling positions) before leaving each pressure level.

1.6 Range of explored variables (proposed test matrix)

Before the execution of the experimental activities aimed at the detection of density wave oscillations and at the definition of steam generator instability regions, system valves have been carefully characterized.

Different values of flow rate have been used to record the concentrated pressure drops corresponding to the various closure positions (test carried out separately for each tube, both at cold and hot conditions). Correlating the results, it was possible to compute the form loss coefficients k at the different valve positions, where the measured pressure drop is simply expressed as:

$$\Delta P = \frac{1}{2} k \rho_{in} V^2 = \frac{1}{2} k \frac{G^2}{\rho_{in}} \quad [1] \qquad (4)$$

Knowledge of valve loss coefficients is of great importance to compute a pre-test analysis, and to refine on that basis a quantitative test campaign matrix (different throttling of inlet valves are in fact very influencing on the instability threshold).

When studying the influence of the inlet subcooling on the limit power (one of the main goals of the experimental campaign), it is preferable then reasoning in terms of per cent values (i.e., as negative x_{in}) rather than in terms of temperatures. Fixed ΔT_{in} correspond in fact to different subcoolings (and different N_{sub} points) in response to remarkable changes of pressure (e.g. from 80 bar to 20 bar).

Therefore, considered all the information provided, a reasonably thorough experimental study of flow instability within two parallel heated tubes requires to examine:

[1] For the sake of simplicity, the considered valve loss coefficients k have been always referred to the fluid velocity within the test section tubes.

- *3 levels of pressure: 80 bar, 40 bar, 20 bar*
- *3 levels of mass flow: in terms of in-tube mass flux, G = 600 kg/sm^2, 400 kg/sm^2, 200 kg/sm^2*
- *at least 2 configurations of V1, V2 inlet valves:*

  k_1= - 1 turn to valve closure (basically open inlet valve configuration, with slight pressure drops introduced);

  k_2= - 2/6 turn to valve closure (partially closed valve configuration, with noticeable pressure drops introduced);

  some runs can be finally carried out with basically closed valves, to demonstrate that risk of parallel channel instability is properly avoided.

- *up to 5 values of inlet subcooling, such as x_{in} = -20%, -15%, -10%,-7.5%, -5%* [2].

The proposed test matrix has been hence built as follows:

Valve Configuration	*Pressure [bar]*	*Mass Flux [kg/sm^2]*	*Subcooling [x_{in}]*
k_1	80	600	-20%
k_1	80	600	-15%
k_1	80	600	-10%
k_1	80	600	-7.5%
k_1	80	600	-5%
k_1	80	400	-20%
k_1	80	400	-15%
k_1	80	400	-10%
k_1	80	400	-7.5%
k_1	80	400	-5%
k_1	80	200	-20%
k_1	80	200	-15%
k_1	80	200	-10%
k_1	80	200	-7.5%
k_1	80	200	-5%
k_1	40	600	-20%
k_1	40	600	-15%
k_1	40	600	-10%
k_1	40	600	-7.5%
k_1	40	600	-5%
k_1	40	400	-20%
k_1	40	400	-15%

[2] Testing all the 5 subcooling values is not actually mandatory for every configuration investigated.

k_1	40	400	-10%
k_1	40	400	-7.5%
k_1	40	400	-5%
k_1	40	200	-20%
k_1	40	200	-15%
k_1	40	200	-10%
k_1	40	200	-7.5%
k_1	40	200	-5%
k_1	20	600	-20%
k_1	20	600	-15%
k_1	20	600	-10%
k_1	20	600	-7.5%
k_1	20	600	-5%
k_1	20	400	-20%
k_1	20	400	-15%
k_1	20	400	-10%
k_1	20	400	-7.5%
k_1	20	400	-5%
k_1	20	200	-20%
k_1	20	200	-15%
k_1	20	200	-10%
k_1	20	200	-7.5%
k_1	20	200	-5%
k_2	80	600	-20%
k_2	80	600	-15%
k_2	80	600	-10%
k_2	80	600	-7.5%
k_2	80	600	-5%
k_2	80	400	-20%
k_2	80	400	-15%
k_2	80	400	-10%
k_2	80	400	-7.5%
k_2	80	400	-5%
k_2	80	200	-20%
k_2	80	200	-15%
k_2	80	200	-10%
k_2	80	200	-7.5%
k_2	80	200	-5%
k_2	40	600	-20%
k_2	40	600	-15%

k_2	40	600	-10%
k_2	40	600	-7.5%
k_2	40	600	-5%
k_2	40	400	-20%
k_2	40	400	-15%
k_2	40	400	-10%
k_2	40	400	-7.5%
k_2	40	400	-5%
k_2	40	200	-20%
k_2	40	200	-15%
k_2	40	200	-10%
k_2	40	200	-7.5%
k_2	40	200	-5%
k_2	20	600	-20%
k_2	20	600	-15%
k_2	20	600	-10%
k_2	20	600	-7.5%
k_2	20	600	-5%
k_2	20	400	-20%
k_2	20	400	-15%
k_2	20	400	-10%
k_2	20	400	-7.5%
k_2	20	400	-5%
k_2	20	200	-20%
k_2	20	200	-15%
k_2	20	200	-10%
k_2	20	200	-7.5%
k_2	20	200	-5%

Resulting on the whole into 90 instability threshold points: for each point, the electrical heating power has to be gradually increased (by small steps) up the detection of flow oscillations.

2 NUMERICAL INVESTIGATION ON BOILING CHANNEL INSTABILITIES WITH RELAP5 CODE

2.1 RELAP5 background

Two different approaches are possible when studying boiling channel instabilities: the development of simplified analytical models, which are able to provide satisfactory explanations of various thermal-hydraulic phenomena, and the

adoption of complex numerical system codes, which permit to provide accurate quantitative predictions. In this frame, the best estimate system code RELAP5 (Reactor Excursion and Leak Analysis Program) was designed for the analysis of all transient and postulated accidents in Light Water Reactor (LWR) systems, including loss-of-coolant accidents (LOCAs) as well as all different types of operational transients. The code is based on a "six-equations" non-homogeneous and non-equilibrium model for the two-phase system, which allows simulating general thermal-hydraulic phenomena.

In the recent years, numerous numerical studies published on DWOs featured the RELAP5 code as the main analysis tool. The majority of works concern with a single boiling channel with an imposed constant pressure drop boundary condition, which is the proper boundary condition to excite the dynamic feedbacks being at the source of the instability mechanism. Among them, Ambrosini and Ferreri [19] performed a detailed analysis about thermal-hydraulic instabilities in a boiling channel using the RELAP5/MOD3.2 code. They investigated a single channel layout with imposed pressures kept constant by two inlet and outlet plena, demonstrating the capability of the RELAP5 system code to detect the onset of DWO instability.

Because of the large amount of literature works already available on the subject, RELAP5 simulations were at first dedicated to the study of a single channel. In particular, we focused on a system configuration in which a large bypass is used to impose the constant pressure drop boundary condition. The bypass solution is typically adopted experimentally to impose the constant pressure drop boundary condition on the single heated channel, as depicted in Figure 6. As a matter of fact, the mass flow rate is forced by an external feedwater pump instead of being driven by the pressure difference across the channel. Besides the capability of the code to detect the onset of instability in the bypass configuration, this work aims at gaining experience in simulating boiling channel instabilities with the RELAP5 code, to correctly approach the preparation of the experimental campaign.

In spite of the lack of publications dedicated to the analysis of DWOs in a parallel channel system with the RELAP5 code, a preliminary study to assess the code behaviour has been performed. Even if more work is needed on the subject, some useful information were derived to preliminary analyse the code capabilities to reproduce boiling channel instabilities in a parallel channel system.

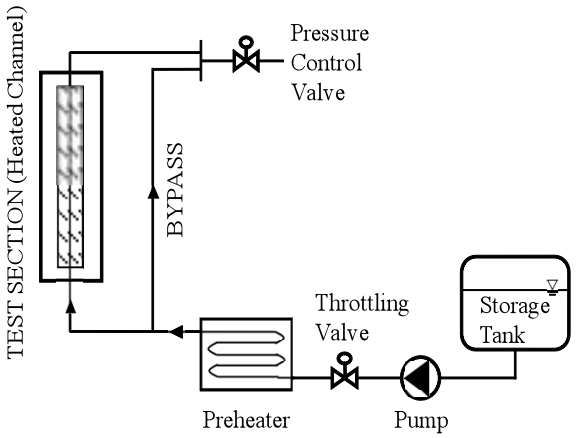

Figure 6 - Typical experimental layout adopted for studying single boiling channel instabilities.

2.2 RELAP5 modelling and numerical setting

Typical setup adopted to simulate DWOs in a single boiling channel is presented in Figure 7-b. A single circular pipe with uniform heating along its axis is connected to two inlet and outlet plena kept at imposed pressures, which let the flow rate adjust at the corresponding steady-state value. During dynamic conditions, perturbations in flow rate are thus allowed to freely evolve towards stable or unstable conditions. Local pressure losses at the inlet and at the outlet of the channel, as well as distributed friction losses, are accounted for. The operating pressures and characteristics of the channel analysed by Ambrosini and Ferreri [19] are inspired to a classical BWR subchannel (Table 2). The same values were considered when addressing the bypass configuration, to make easier a comparison of simulation results.

As concerns the bypass configuration, a large bypass tube is connected to the heated test channel, to guarantee a constant pressure drop across the channel. The layout is modelled with the RELAP5/MOD3.3 code connecting two pipe components of different diameter by means of two branches (Figure 7-a). The mass flow rate is provided by a time-dependent junction, connected directly to the lower branch. Inlet pressure and temperature are fixed using a time-dependent volume. Outlet pressure is imposed by another time-dependent volume connected to the upper branch by means of a single junction. Local pressure loss coefficients k_{in} and k_{ex} are introduced on the four connections between branches and pipe components, and simulate the presence of inlet and exit throttling. Pressure drop across the channel is imposed by the exit pressure, the mass flow rate and the characteristic of the channel.

Table 2 - RELAP5 simulation parameters.

Heated Channel	
Diameter [m]	0.0124
Length [m]	3.658
Roughness [m]	$2.5 \cdot 10^{-5}$
Operating parameters	
Exit pressure [Pa]	$7.0 \cdot 10^{6}$
Inlet temperatures [°C]	151.3 - 282.3
k_{in}	23
k_{ex}	5

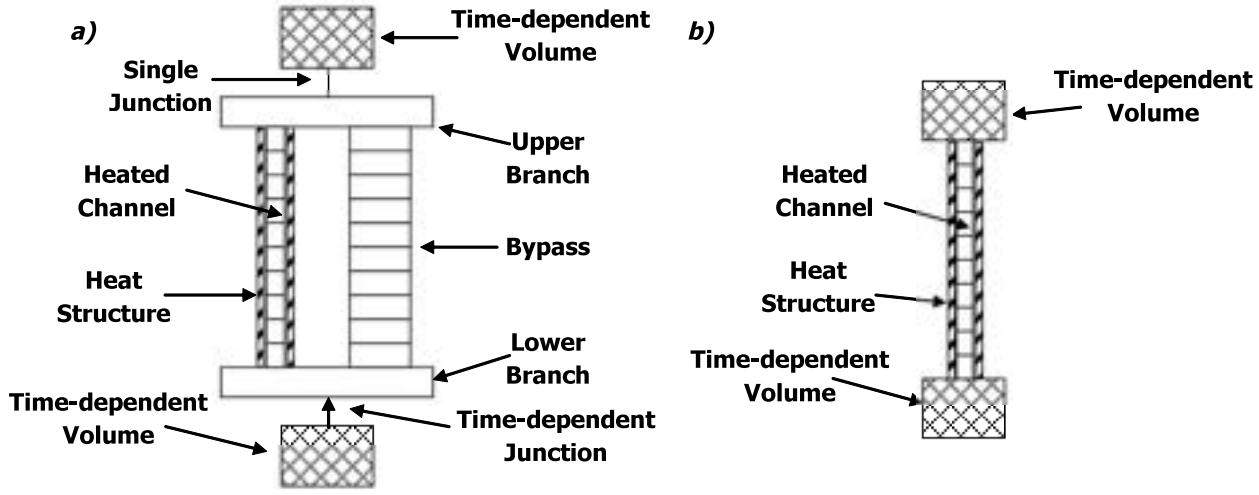

Figure 7 - RELAP5 nodalization in the two different configurations:

a) with a bypass tube; *b)* with a single channel alone.

The heated channel is subdivided in 48 nodes as in [19], to meet a better comparison of the results. The number of nodes is also selected following other remarks which will be discussed later. Imposed heat flux condition is adopted. The heat structures wherein power generation is accounted are assumed very thin and present high thermal conductivity and low heat capacity to avoid distortions in the imposed thermal flux condition, and to neglect tube wall dynamic behaviour as well. As far as the bypass ratio ($R_{by}=A_{by}/A_{hc}$) is concerned, the initial value of the bypass diameter is assumed equal to 10 times the diameter of the heated channel ($R_{by}=100$), in order to ensure the constant pressure drop boundary condition.

The following procedure is adopted to reach the instability boundary for the different operating conditions: at the beginning of each run specific values of exit pressure, mass flow rate and inlet water temperature are selected as initial conditions. Flow circulation in the system starts at zero power, then power generation in the heat structures is increased gradually till the unstable condition is reached. The increase rate is higher at the beginning of the transient, to quickly approach the unstable region, then it is lowered to guarantee an easier detection of the onset of instability.

Ambrosini and Ferreri [19] performed a large number of calculations to analyze the effect on the results of the different models available in the code, as well as the nodalization and the numerical scheme. Their results were considered the starting point for the analysis in presence of the bypass, in which the same models and numerical settings are adopted.

The UVUT (Unequal Velocities Unequal Temperatures) model is adopted, because it is found to be more robust and reliable when compared with the EVET (Equal Velocities Equal Temperatures) model, which is indeed more conservative [19]. The semi-implicit numerical scheme is selected. Calculations rarely crash due to numerical problems, and the introduction of numerical diffusion is limited with respect to the nearly-implicit numerical scheme [19]. To reduce as much as possible the amount of numerical diffusion introduced also with the semi-implicit discretization, a control variable which forces the time step to remain equal to a fixed value of the Courant number has been developed:

$$\Delta t = 0.95 \cdot \Delta t_{Cou} \tag{5}$$

Finally, a number of nodes equal to 48 is selected as in [19]. Smoother prediction of the stability boundary is assured also in the case of the UVUT model, even though it is less sensitive to variations of the number of nodes.

2.3 Results

The first set of data were collected adopting a bypass ratio $R_{by}=100$ and exploring different inlet temperatures. Figure 8 shows a comparison between the maps obtained with the bypass tube and with the single heated channel.

The pressure drop across the heated channel was taken equal in the two different scenarios. The presence of a large bypass tube does not influence the onset of instability and only small deviations are observed at very low subcooling numbers.

It is important to notice that the criterion to detect the appearance of DWOs is not an exact one, thus it is expected to affect the results introducing some uncertainty. The stability boundary has been detected by the appearance of growing oscillations in the mass flow rate through the heated channel (Figure 9). The system was considered unstable when the oscillations appeared fully developed.

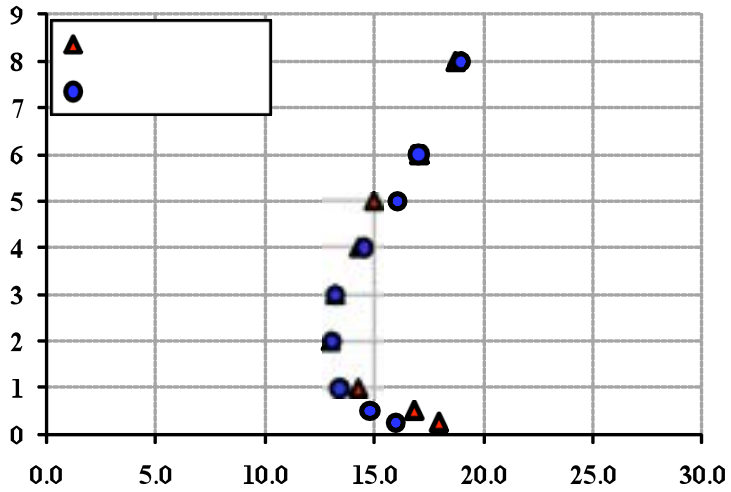

Figure 8 - Stability map calculated with the bypass tube ($R_{by}=100$) compared with the stability map obtained in a single channel with imposed pressure drop.

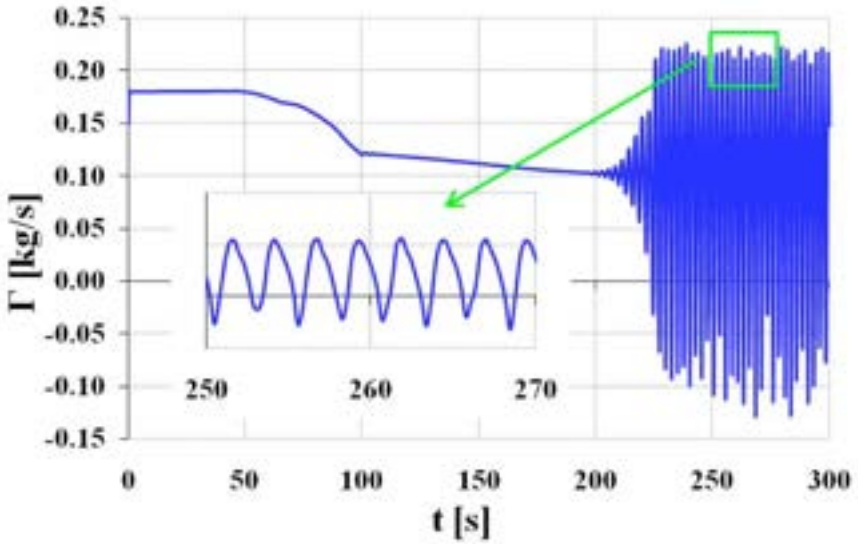

Figure 9 - Mass flow rate behaviour in the heated channel during a simulation performed with $N_{sub}=4$.

In accordance with literature results [1], the effect of the inlet subcooling on system stability is found to be stabilizing at high subcoolings and destabilizing at low subcoolings. The results of the single channel alone simulations show also a fair agreement with the ones obtained in [19].

The period of oscillations, which is known from literature to grow with the subcooling number, is correctly reproduced by the RELAP5 code with the bypass configuration, as it is shown in Figure 10. The ratio between the period of oscillations and the transit time in the two configurations (single channel alone and with the bypass) is depicted. As expected, this ratio increases with higher inlet subcoolings [19].

The transit time in Figure 10 was calculated with a proper control variable developed in RELAP5, defined as the ratio between the total mass of water and steam in the heated channel and the mass flow rate.

$$t = \frac{\sum_{i=1}^{48} m}{\Gamma} \tag{6}$$

Moreover, the transit time of the mixture in homogeneous flow is given by:

$$t = \Delta t_1 + \Delta t_2 = \frac{\rho_f \cdot \Delta h_{in}}{q'''} + \frac{h_{fg}}{q''' \cdot v_{fg}} \cdot ln\left(1 + \frac{v_{fg}}{v_f} \cdot x_{ex}\right) \tag{7}$$

As it is shown in Figure 11, the two different expressions show the same trend. The analytical transit time is constantly 0.1 s lower than the value calculated with RELAP5.

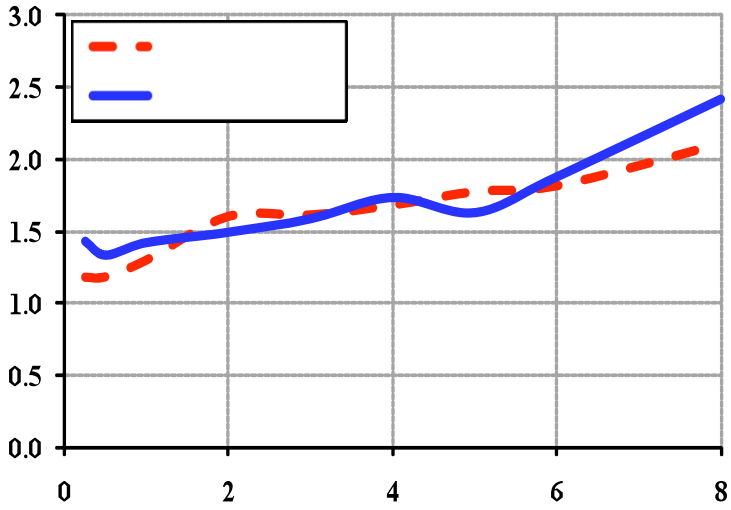

Figure 10 - Ratio between the period of oscillations and the transit time in the heated channel with and without the bypass tube.

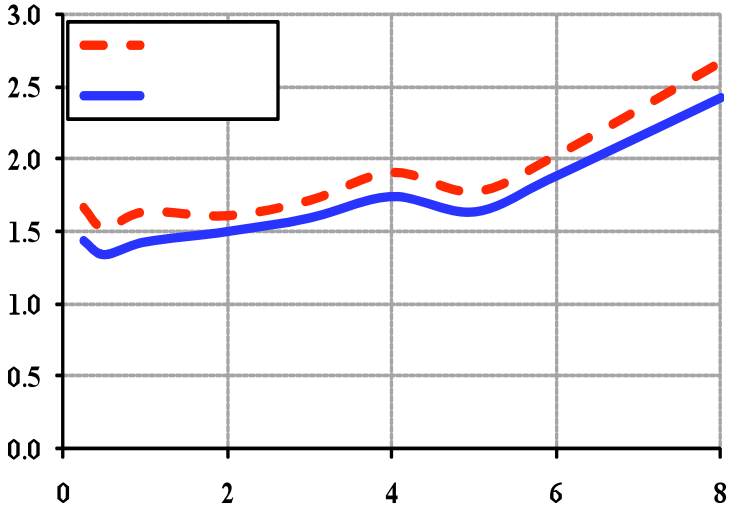

Figure 11 - Ratio between the period of oscillations and the transit time in the heated channel calculated with the analytical expression and with the RELAP5 control variable (with bypass configuration).

2.3.1 Sensitivity study on bypass ratio

The influence of the bypass area on system stability has been investigated performing a sensitivity analysis on the bypass ratio. Bypass ratio was at first reduced to find out the value required to guarantee a constant pressure drop across the heated channel. The results are presented in Figure 12. Halving the bypass ratio ($R_{by}=50$) does not modify the stability of the heated channel. On the contrary, further reduction tends to render the system more stable (stability curves shifted to the right in the N_{pch}-N_{sub} space).

Stable region becomes larger when the bypass ratio is reduced to 20, except for low inlet subcoolings, for which the stability boundary is rather unchanged. A last reduction to 10 remarkably widens the stability region. Hence, a bypass ratio at least equal to 20 is needed to maintain properly the constant pressure drop boundary condition.

Increasing the bypass ratio (up to 200 and 500 respectively) does not affect significantly the stability of the system. As it is shown in Figure 13, the stability is independent on the bypass ratio for sufficiently large values.

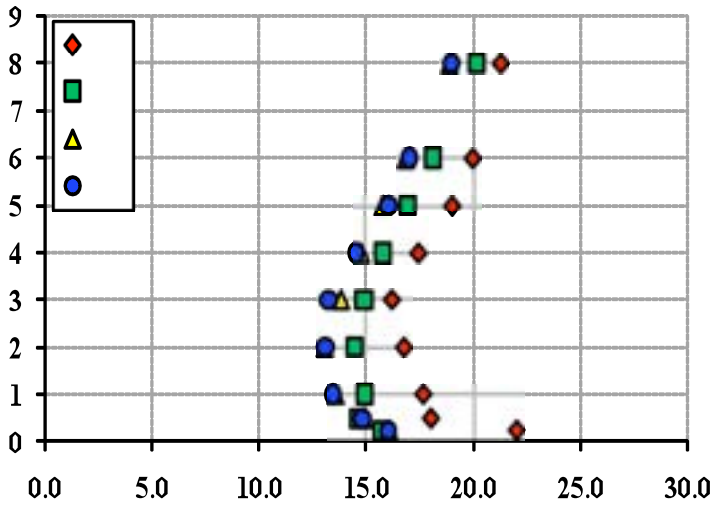

Figure 12 - Stability maps obtained with different values of the bypass ratio R_{by} (respectively 100, 50, 20 and 10).

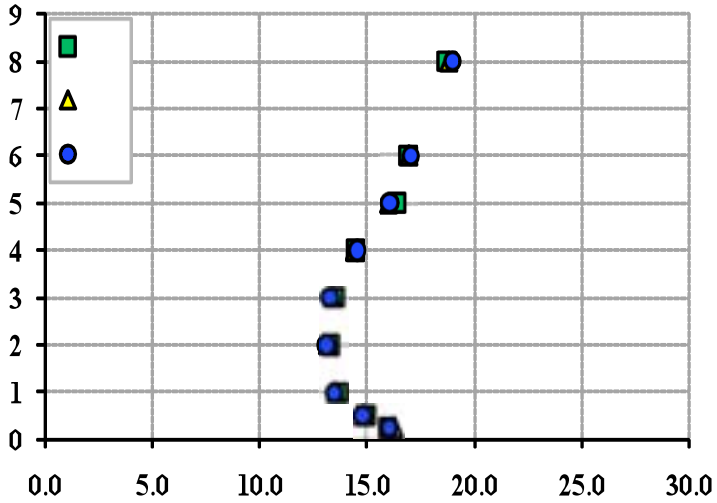

Figure 13 - Stability maps obtained with different values of the bypass ratio R_{by} (respectively 100, 200 and 500).

2.4 Preliminary calculations on parallel channel instabilities

A preliminary study about DWOs in a parallel channel system was made simulating with the RELAP5 code the experimental test section located at SIET labs. The same nodalization developed for the bypass case permitted to easily model the experimental facility only modifying the geometrical parameters of the two channels. The twin channels, simulated with two pipe components, are connected with two upper and lower branches. They are inclined to match the height of the test facility, in which the tubes are helically coiled. Pipe components are heated for the first 24 m, where uniform imposed heat flux is considered. The heated length is subdivided in 48 nodes. In the last 8 m, which represent the riser section, no heat is supplied. 8 nodes constitute the riser section. Inlet pressure and temperature are fixed using a time-dependent volume, whereas the mass flow rate is imposed by a time-dependent junction. Local pressure loss coefficients k_{in} are introduced on the two connections between lower branches and pipe components, to simulate the presence of inlet valves, namely V1 and V2 in Figure 5. Also the two valves V3 and V4, located respectively before the lower branch and after the upper branch, are simulated, although they seem to have no influence on the system stability. Twin channel characteristics are resumed in Table 3.

Table 3 - RELAP5 twin channels parameters.

Channel Parameters	
Heated Length [m]	24
Riser Length [m]	8
Total Length [m]	32
Height [m]	8
Diameter [cm]	1.25
Inclination Angle [°]	14.48
Roughness [m]	$3.08 \cdot 10^{-6}$

Preliminary simulations explored different inlet subcoolings for fixed values of system pressure, mass flow rate and inlet throttling (Table 4).

Table 4 - RELAP5 system parameters.

System Parameters	
Inlet Temperatures [°C]	175.43 – 250.27
Exit Pressure [MPa]	4
Mass Flow Rate [kg/h]	261
k_{in}	20

The stability map is shown in Figure 14. The onset of instability is found for values of the phase change number N_{pch} which are higher if compared with the results obtained in single channel configuration. On the other hand, they are consistent with the system stabilization obtained reducing the bypass ratio in Par.2.3.1. Moreover, the effect of subcooling seems to be always stabilizing, except for very low subcooling numbers, at which only a slight destabilization effect is observed.

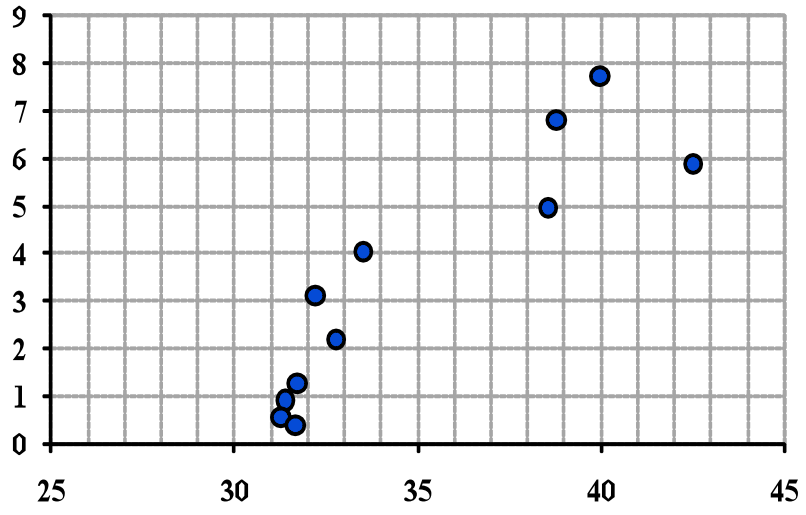

Figure 14 - Stability map calculated with parallel channels using the parameters resumed in Table 3 and Table 4.

The study on RELAP5 code capabilities to correctly reproduce DWOs in a parallel channel system is far from completion and is currently underway. More work is needed focusing on different values of system pressure, mass flow rate and valve position. In addition, a sensitivity analysis is required to investigate the effect on results of various code models and settings, in particular concerning the nodalization. All these issues will be fully addressed after the completion of the experimental campaign at SIET labs.

3 PRE-TEST ANALYSIS WITH ANALYTICAL LUMPED PARAMETER MODEL

This Section describes the development of an analytical dynamic model aimed at a theoretical prediction of the instability thresholdsbes. Realized modelling is based on the work of Muñoz-Cobo et al. [20], who studied out-of-phase oscillations (DWO kind) between parallel channels of distinct core regions of a BWR reactor. Proper modifications have been introduced to fit the modelling approach with steam generator tubes with imposed thermal power (representative of the experimental facility conditions).

The developed model is based on a lumped approach (0-D) for the two zones characterizing a single boiling channel, that are single-phase region and two-phase region, divided by the boiling boundary (where the fluid reaches saturation temperature). Differential conservation equations of mass and energy are considered for each region, whereas momentum equation is integrated along the whole channel. Wall dynamics is accounted for in the two regions following lumped wall temperature dynamics by means of the respective heat transfer balances. Instability can be studied both for a single boiling channel and for two parallel channels. The respective boundary conditions are introduced as closure relationships, i.e. constant-pressure-drop (ΔP = const) for the single channel, and equal-pressure-drop (same $\Delta P(t)$) for the two parallel channels. The main hypotheses of the provided modelling are:

a) homogenous two-phase flow model;
b) uniform heating along the channel (linear increase of quality with tube abscissa *z*);
c) system of constant pressure (pressure term is neglected within the energy equation).

3.1 Mathematical modelling

Modelling equations are derived by the continuity of mass and energy for a single-phase fluid and a two-phase fluid, respectively.

Single-phase flow equations read:

$$\frac{\partial \rho}{\partial t} + \frac{\partial G}{\partial z} = 0 \tag{8}$$

$$\frac{\partial (\rho h)}{\partial t} + \frac{\partial (G h)}{\partial z} = Q''' \tag{9}$$

Two-phase mixture is dealt according to homogeneous flow model. By defining the homogeneous density ρ_H and the reaction frequency Ω [4][21] as follows:

$$\rho_H = \rho_f (1 - \bar{\alpha}) + \rho_g \bar{\alpha} = \frac{1}{v_f + \bar{x} v_{fg}} \tag{10}$$

$$\Omega(t) = \frac{Q(t) v_{fg}}{A H h_{fg}} \tag{11}$$

one gets:

$$\frac{\partial \rho_H}{\partial t} + \frac{\partial G}{\partial z} = 0 \tag{12}$$

$$\frac{\partial j}{\partial z} = \Omega(t) \tag{13}$$

Momentum equation is then accounted for by integrating the pressure balance along the channel:

$$\int_0^H \frac{\partial G(z,t)}{\partial t} dz = \Delta P(t) - \Delta P_{acc} - \Delta P_{grav} - \Delta P_{frict} \tag{14}$$

3.1.1 Mass-energy model in the two-phase region

The continuity equation for a homogeneous two-phase mixture – Eq.(13) – is integrated to calculate the average mass flux $\langle G_{2\phi} \rangle$ in the two-phase region (to be used for the calculation of two-phase frictional pressure drops). The well known expression of the total volumetric flux is reminded:

$$j = \left(\frac{x}{\rho_g} + \frac{1-x}{\rho_f} \right) G_{2\phi}(z,t) \tag{15}$$

Integrating Eq.(10) from the boiling boundary position $z_{BB}(t)$ to an arbitrary position z, and accounting for Eq.(15), one obtains after some algebra:

$$G_{2\phi}(z,t) = \frac{\Omega(t)\left[z - z_{BB}(t)\right] + v_f G_{in}(t)}{v_f + x(z,t) v_{fg}} \tag{16}$$

Eq.(16) can be then used to calculate the mass flux at channel exit G_{ex} (with $z=H$), and the average mass flux in the two-phase region $\langle G_{2\phi} \rangle$ (by applying the theorem of integral average):

$$G_{ex} = \frac{\Omega\left[H - z_{BB}\right] + v_f G_{in}}{v_f + x_{ex} v_{fg}} \tag{17}$$

$$\langle G_{2\phi} \rangle = \frac{1}{H - z_{BB}} \int_{z_{BB}}^{H} G_{2\phi}(z,t) dz = \frac{\Omega\left[H - z_{BB}\right]}{x_{ex} v_{fg}} + \frac{v_f}{x_{ex} v_{fg}} \left(G_{in} - \frac{\Omega\left[H - z_{BB}\right]}{x_{ex} v_{fg}} \right) \ln\left(1 + \frac{v_{fg}}{v_f} x_{ex} \right) \tag{18}$$

3.1.2 Integration of momentum equation

Within Eq.(14), $\Delta P(t)$ is the difference between the inlet and outlet channel pressure:

$$\Delta P(t) = P_{in} - P_{ex} \tag{19}$$

The accelerative term of pressure drops ΔP_{acc} can be represented as:

$$\Delta P_{acc} = G_{ex}^2 \left[\frac{x_{ex}^2}{\alpha_{ex} \rho_g} + \frac{(1 - x_{ex})^2}{(1 - \alpha_{ex}) \rho_f} \right] - \frac{G_{in}^2}{\rho_f} \tag{20}$$

The gravitational term of pressure drops ΔP_{grav} can be represented as:

$$\Delta P_{grav} = g\rho_f z_{BB} + g\left(1-\bar{\alpha}\right)\rho_f\left[H - z_{BB}\right] + g\bar{\alpha}\rho_g\left[H - z_{BB}\right] \tag{21}$$

The frictional term of pressure drops ΔP_{frict} can be represented as:

$$\Delta P_{frict} = \left(k_{in} + f\frac{z_{BB}}{D}\right)\frac{G_{in}^2}{2\rho_f} + f\frac{H - z_{BB}}{D}\left\langle\Phi^2\right\rangle\frac{\left\langle G_{2\phi}\right\rangle^2}{2\rho_f} + k_{ex}\Phi_{ex}^2\frac{G_{ex}^2}{2\rho_f} \tag{22}$$

single-phase (concentrated at inlet + distributed) — *two-phase distributed* — *two-phase concentrated at outlet*

Left hand side term of the pressure drop balance – Eq.(14) – is treated by splitting the integration into two intervals, from *0* to the boiling boundary z_{BB}, and from z_{BB} to the channel length *H*, and applying for the second interval the Leibniz rule:

$$\int_0^H \frac{\partial G}{\partial t}dz = z_{BB}\frac{dG_{in}}{dt} + \frac{d}{dt}\int_{z_{BB}}^H G_{2\phi}dz + G_{in}\frac{dz_{BB}}{dt} \tag{23}$$

Mass flux integral along two-phase region is computed according to Eq.(18), giving:

$$\frac{d}{dt}\int_{z_{BB}}^H G_{2\phi}dz = b_1\frac{dz_{BB}}{dt} + b_2\frac{dx_{ex}}{dt} + b_3\frac{dG_{in}}{dt} + b_4\frac{d\Omega}{dt} \tag{24}$$

where the following coefficients are defined:

$$b_1 = \frac{-2\Omega\left[H - z_{BB}\right]}{x_{ex}v_{fg}} + \ln\left(1 + \frac{v_{fg}}{v_f}x_{ex}\right)\frac{v_f}{v_{fg}x_{ex}}\left(\frac{2\Omega\left[H - z_{BB}\right]}{v_{fg}x_{ex}} - G_{in}\right) \tag{25}$$

$$b_2 = \frac{-\Omega\left[H - z_{BB}\right]^2}{v_{fg}x_{ex}^2} + \frac{v_f\left[H - z_{BB}\right]}{v_{fg}x_{ex}^2}\ln\left(1 + \frac{v_{fg}}{v_f}x_{ex}\right)\left(\frac{2\Omega\left[H - z_{BB}\right]}{v_{fg}x_{ex}} - G_{in}\right) + \ldots$$
$$\ldots\frac{v_f\left[H - z_{BB}\right]}{x_{ex}\left(v_f + v_{fg}x_{ex}\right)}\left(G_{in} - \frac{\Omega\left[H - z_{BB}\right]}{x_{ex}v_{fg}}\right) \tag{26}$$

$$b_3 = \frac{v_f\left[H - z_{BB}\right]}{v_{fg}x_{ex}}\ln\left(1 + \frac{v_{fg}}{v_f}x_{ex}\right) \tag{27}$$

$$b_4 = \frac{\left[H - z_{BB}\right]^2}{v_{fg}x_{ex}}\left(1 - \frac{v_f}{v_{fg}x_{ex}}\ln\left(1 + \frac{v_{fg}}{v_f}x_{ex}\right)\right) \tag{28}$$

Finally, the equation governing the rate of change of mass flux at the inlet of the channel is obtained substituting Eq.(24) into Eq.(14):

$$\left(b_3 + z_{BB}\right)\frac{dG_{in}}{dt} = \Delta P(t) - \Delta P_{acc} - \Delta P_{grav} - \Delta P_{frict} - \left(G_{in} + b_1\right)\frac{dz_{BB}}{dt} - b_2\frac{dx_{ex}}{dt} - b_4\frac{d\Omega}{dt} \tag{29}$$

This equation permits to know the dynamics of the flow rate entering the respective channel, once they are defined:

i. the dynamics of the boiling boundary z_{BB};
ii. the dynamics of the exit quality x_{ex};
iii. the dynamics of the reaction frequency Ω (from heated wall model);

3.1.3 Boiling boundary dynamics

Boiling boundary dynamics can be easily obtained by integrating the energy equation – Eq.(9) – in the single-phase region [14]:

$$\int_0^{z_{BB}} \left[\frac{Q}{V_{ch}} - \frac{\partial(Gh)}{\partial z} \right] dz = \int_0^{z_{BB}} \frac{\partial(\rho h)}{\partial t} dz \tag{30}$$

Leibniz rule is applied to the right hand size term of Eq.(30). The strong hypothesis that local enthalpy changes simultaneously at all the axial locations (with average value $h = (h_{in} + h_f)/2$) is assumed. It is just mentioned that this approximation is reasonable at low frequency.
Integrating Eq.(30) and after some algebra, one obtains:

$$\frac{dz_{BB}}{dt} = \frac{2G_{in}}{\rho_f} - \frac{2Qz_{BB}}{(h_f - h_{in})V_{ch}\rho_f} = b_8 \tag{31}$$

3.1.4 Exit quality dynamics

Exit quality dynamics is obtained from the formula that relates the void fraction α to the quality, with homogenous flow model:

$$\alpha = \frac{\gamma x}{1 + (\gamma - 1)x} \tag{32}$$

where:

$$\gamma = \frac{v_g}{v_f} = \frac{\rho_f}{\rho_g} \tag{33}$$

The average void fraction $\overline{\alpha}$ is computed as:

$$\overline{\alpha} = \frac{1}{x_{ex}(t)} \int_0^{x_{ex}(t)} \alpha dx = \frac{\gamma}{\gamma - 1} \left[1 - \frac{1}{(\gamma - 1)x_{ex}} \ln(1 + (\gamma - 1)x_{ex}) \right] \tag{34}$$

If Eq.(34) is derived with respect to time, and two-phase mass conservation equation – Eq.(12) –is integrated along the boiling region, one has:

$$\frac{d\overline{\alpha}}{dt} = b_5 \frac{dx_{ex}}{dt} \tag{35}$$

$$\frac{d\bar{\alpha}}{dt} = \frac{G_{in} - G_{ex}}{\left(\rho_g - \rho_f\right)\left[H - z_{BB}\right]} + \frac{\bar{\alpha}}{H - z_{BB}} \frac{dz_{BB}}{dt} \tag{36}$$

with:

$$b_5 = \frac{\gamma}{(\gamma-1)^2 x_{ex}} \left[- \frac{(\gamma-1)}{1+(\gamma-1)x_{ex}} + \frac{\ln\left(1+(\gamma-1)x_{ex}\right)}{x_{ex}} \right] \tag{37}$$

Rearranging Eqs.(34), (35), (36), the dynamics of the exit quality is finally obtained:

$$\frac{dx_{ex}}{dt} = b_9 \tag{38}$$

where:

$$b_9 = b_6 + b_7 b_8 \tag{39}$$

with:

$$b_6 = \frac{G_{in} v_{fg} x_{ex} - \Omega\left[H - z_{BB}\right]}{\left[H - z_{BB}\right]\left(v_f + v_{fg} x_{ex}\right) \rho_{fg} b_5} \tag{40}$$

$$b_7 = \frac{\gamma}{(\gamma-1)\left[H - z_{BB}\right] b_5} \left[1 - \frac{\ln\left(1+(\gamma-1)x_{ex}\right)}{(\gamma-1)x_{ex}} \right] \tag{41}$$

3.1.5 Reaction frequency dynamics

The reaction frequency dynamics is given as:

$$\frac{d\Omega}{dt} = b_{10} = \frac{v_{fg}}{h_{fg}} \frac{1}{AH} \frac{dQ}{dt} \tag{42}$$

thus, it depends on the model adopted for the heated wall.

In this model, a lumped two-region approach is chosen; heated wall dynamics is evaluated separately for single-phase and two-phase regions, following the dynamics of the respective wall temperatures according to a heat transfer balance:

$$\frac{dQ^{1\phi}}{dt} = M_h^{1\phi} c_h \frac{dT_h^{1\phi}}{dt} = Q^{1\phi} - (hS)^{1\phi}\left(T_h^{1\phi} - T_{fl}^{1\phi}\right) \tag{43}$$

$$\frac{dQ^{2\phi}}{dt} = M_h^{2\phi} c_h \frac{dT_h^{2\phi}}{dt} = Q^{2\phi} - (hS)^{2\phi}\left(T_h^{2\phi} - T_{fl}^{2\phi}\right) \tag{44}$$

Heated wall dynamics is governed by the following two coefficients (single-phase and two-phase wall portion, respectively):

$$b_{10}^{1\phi} = \frac{1}{M_h^{1\phi} c_h} \left[Q^{1\phi} - (hS)^{1\phi}\left(T_h^{1\phi} - T_{fl}^{1\phi}\right) \right] \tag{45}$$

$$b_{10}^{2\phi} = \frac{1}{M_h^{2\phi} c_h}\left[Q^{2\phi} - (hS)^{2\phi}\left(T_h^{2\phi} - T_{fl}^{2\phi}\right)\right] \tag{46}$$

Combining Eqs.(43), (44), and rearranging into Eq.(42), one has:

$$b_{10} = \frac{v_{fg}}{h_{fg}}\frac{1}{AH}\left[M_h^{1\phi} c_h b_{10}^{1\phi} + M_h^{2\phi} c_h b_{10}^{2\phi}\right] \tag{47}$$

In the above equations, specific empirical correlations are considered to calculate single-phase and two-phase heat transfer coefficients, respectively the Dittus-Boelter and the Kandlikar equation [22].

3.2 Model development

3.2.1 Definition of the boundary conditions

Model construction is based on the ordinary differential equations drawn in Section 3.1, and descriptive of the hydraulic and thermal behaviour of a single boiling channel. When the instability within a single channel is of interest, boundary condition of constant pressure drop *ΔP(t)* between channel inlet and outlet must be simply introduced within the momentum balance equation – Eq.(29) –.

Parallel channel instability (for the two parallel channels object of this study) is dealt imposing: *(i)* the same pressure drop dependence with time across the two channels; *(ii)* a constant total flow rate:

$$\Delta P_1(t) = \Delta P_2(t) = \Delta P(t) \tag{48}$$

$$G_{in,1}(t) = G_{in,2}(t) = constant \tag{49}$$

Deriving with time the second boundary condition – Eq.(49) –:

$$\frac{dG_{in,1}}{dt} = -\frac{dG_{in,2}}{dt} \tag{50}$$

When working with two parallel channels, the complete set of ODEs defined in Section 3.1 has to be written for each of the two channels. Boundary conditions are accounted for within the momentum equations. Writing down Eq.(29) for the two channels separately, one has:

$$\left(b_{3,1} + z_{BB,1}\right)\frac{dG_{in,1}}{dt} = \Delta P(t) - \Delta P_{acc,1} - \Delta P_{grav,1} - \Delta P_{frict1} - \left(G_{in,1} + b_{1,1}\right)b_{8,1} - b_{2,1}b_{9,1} - b_{4,1}b_{10,1} \tag{51}$$

$$\left(b_{3,2} + z_{BB,2}\right)\frac{dG_{in,2}}{dt} = \Delta P(t) - \Delta P_{acc,2} - \Delta P_{grav,2} - \Delta P_{frict2} - \left(G_{in,2} + b_{1,2}\right)b_{8,2} - b_{2,2}b_{9,2} - b_{4,2}b_{10,2} \tag{52}$$

Subtracting Eq.(52) from Eq.(51), and considering the boundary condition Eq.(50), the dynamics of the mass flux entering channel 1 is finally obtained:

$$\left(b_{3,1}+z_{BB,1}+b_{3,2}+z_{BB,2}\right)\frac{dG_{in,1}}{dt}=\Delta P_{acc,2}-\Delta P_{acc,1}+\Delta P_{grav,2}-\Delta P_{grav,1}+\Delta P_{frict2}-\Delta P_{frict1}+\ldots$$
$$\ldots\left(G_{in,2}+b_{1,2}\right)b_{8,2}-\left(G_{in,1}+b_{1,1}\right)b_{8,1}+b_{2,2}b_{9,2}-b_{2,1}b_{9,1}+b_{4,2}b_{10,2}-b_{4,1}b_{10,1} \quad (53)$$

$$\frac{dG_{in,1}}{dt}=b_{11,1} \quad (54)$$

where:

$$b_{11,1}=\frac{1}{\left[b_{3,1}+z_{BB,1}+b_{3,2}+z_{BB,2}\right]}\left\{\begin{array}{l}\left(\Delta P_{acc,2}-\Delta P_{acc,1}\right)+\left(\Delta P_{grav,2}-\Delta P_{grav,1}\right)+\left(\Delta P_{frict2}-\Delta P_{frict1}\right)+\ldots\\ \ldots\left(G_{in,2}+b_{1,2}\right)b_{8,2}-\left(G_{in,1}+b_{1,1}\right)b_{8,1}+b_{2,2}b_{9,2}-b_{2,1}b_{9,1}+b_{4,2}b_{10,2}-b_{4,1}b_{10,1}\end{array}\right\} \quad (55)$$

At the end, the previous equations can be also rearranged to obtain a compact explicit expression for the pressure drop *ΔP(t)*. Dividing Eqs.(51), (52) by $\left(b_{3,1}+z_{BB,1}\right)$ and $\left(b_{3,2}+z_{BB,2}\right)$ respectively, and summing the resulting equations, after some calculus one has:

$$\Delta P(t)=w_1\Delta P_{acc,1}+w_1\Delta P_{grav,1}+w_1\Delta P_{frict1}+w_1F_1+w_1B_1+w_2\Delta P_{acc,2}+w_2\Delta P_{grav,2}+w_2\Delta P_{frict2}+w_2F_2+w_2B_2 \quad (56)$$

where the following terms are defined for each channel *(i = 1,2)*:

$$F_i=\left(G_{in,i}+b_{1,i}\right)b_{8,i} \quad (57)$$

$$B_i=b_{2,i}b_{9,i}+b_{4,i}b_{10,i} \quad (58)$$

$$w_i=\frac{\dfrac{1}{b_{3,i}+z_{BB,i}}}{\dfrac{1}{b_{3,1}+z_{BB,1}}+\dfrac{1}{b_{3,2}+z_{BB,2}}} \quad (59)$$

3.2.2 Summary of the modelling equations

With respect to two parallel channels case (which is the system analyzed in the present work), the comprehensive model is comprised of a set of 9 ordinary differential equations, in the form of:

$$\frac{dy_i}{dt}=f_i(y) \qquad i = 1, 2, ..., 9 \quad (60)$$

where the state variables are:

$$y_1=z_{BB,1} \quad y_2=z_{BB,2} \quad y_3=x_{ex,1} \quad y_4=x_{ex,2} \quad y_5=G_{in,1}$$
$$y_6=T_{h,1}^{1\phi} \quad y_7=T_{h,1}^{2\phi} \quad y_8=T_{h,2}^{1\phi} \quad y_9=T_{h,2}^{2\phi} \quad (61)$$

For the aims of the developed model, thermal power (Q_1, Q_2), inlet loss coefficient ($k_{in,1}$, $k_{in,2}$), and exit loss coefficient ($k_{ex,1}$, $k_{ex,2}$) for the two distinct channels are defined as system inputs.[3]

[3] It is just mentioned that in case of single boiling channel modelling, also the imposed *ΔP(t)* must be defined as system input.

For the sake of clarity, all the coefficients introduced within the modelling equations – with respective meanings – are reported in Table 5.

Table 5 – List of the coefficients defined throughout the development of the modelling equations.

$b_1 = \frac{-2\Omega[H-z_{BB}]}{x_{ex}v_{fg}} + \ln\left(1+\frac{v_{fg}}{v_f}x_{ex}\right)\frac{v_f}{v_{fg}x_{ex}}\left(\frac{2\Omega[H-z_{BB}]}{v_{fg}x_{ex}} - G_{in}\right)$
relates the dynamics of the boiling boundary to the dynamics of two-phase mass flux (integral)
$b_2 = \frac{-\Omega[H-z_{BB}]^2}{v_{fg}x_{ex}^2} + \frac{v_f[H-z_{BB}]}{v_{fg}x_{ex}^2}\ln\left(1+\frac{v_{fg}}{v_f}x_{ex}\right)\left(\frac{2\Omega[H-z_{BB}]}{v_{fg}x_{ex}} - G_{in}\right) + \ldots$ $\ldots\frac{v_f[H-z_{BB}]}{x_{ex}(v_f+v_{fg}x_{ex})}\left(G_{in} - \frac{\Omega[H-z_{BB}]}{x_{ex}v_{fg}}\right)$
relates the dynamics of the exit quality to the dynamics of two-phase mass flux (integral)
$b_3 = \frac{v_f[H-z_{BB}]}{v_{fg}x_{ex}}\ln\left(1+\frac{v_{fg}}{v_f}x_{ex}\right)$
relates the dynamics of inlet mass flux to the dynamics of two-phase mass flux (integral)
$b_4 = \frac{[H-z_{BB}]^2}{v_{fg}x_{ex}}\left(1-\frac{v_f}{v_{fg}x_{ex}}\ln\left(1+\frac{v_{fg}}{v_f}x_{ex}\right)\right)$
relates the dynamics of the reaction frequency to the dynamics of two-phase mass flux (integral)
$b_5 = \frac{\gamma}{(\gamma-1)^2 x_{ex}}\left[-\frac{(\gamma-1)}{1+(\gamma-1)x_{ex}} + \frac{\ln(1+(\gamma-1)x_{ex})}{x_{ex}}\right]$
relates the dynamics of the exit quality to the dynamics of the average void fraction
$b_6 = \frac{G_{in}v_{fg}x_{ex} - \Omega[H-z_{BB}]}{[H-z_{BB}](v_f+v_{fg}x_{ex})\rho_{fg}b_5}$
coefficient within exit quality dynamics
$b_7 = \frac{\gamma}{(\gamma-1)[H-z_{BB}]b_5}\left[1-\frac{\ln(1+(\gamma-1)x_{ex})}{(\gamma-1)x_{ex}}\right]$
coefficient within exit quality dynamics
$b_8 = \frac{2G_{in}}{\rho_f} - \frac{2Qz_{BB}}{(h_f-h_{in})\gamma_{ch}\rho_f}$
boiling boundary dynamics
$b_9 = b_6 + b_7 b_8$
exit quality dynamics
$b_{10} = \frac{v_{fg}}{h_{fg}}\frac{1}{AH}\frac{dQ}{dt}$
reaction frequency dynamics

$$b_{10}^{1\phi} = \frac{1}{M_h^{1\phi} c_h}\left[Q^{1\phi} - (hS)^{1\phi}\left(T_h^{1\phi} - T_{fl}^{1\phi}\right)\right]$$

dynamics of wall temperature in the single-phase region

$$b_{10}^{2\phi} = \frac{1}{M_h^{2\phi} c_h}\left[Q^{2\phi} - (hS)^{2\phi}\left(T_h^{2\phi} - T_{fl}^{2\phi}\right)\right]$$

dynamics of wall temperature in the two-phase region

$$b_{11,1} = \frac{1}{\left[b_{3,1} + z_{BB,1} + b_{3,2} + z_{BB,2}\right]}\left\{\begin{array}{l}\left(\Delta P_{acc,2} - \Delta P_{acc,1}\right) + \left(\Delta P_{grav,2} - \Delta P_{grav,1}\right) + \left(\Delta P_{frict2} - \Delta P_{frict1}\right) + \ldots \\ \ldots\left(G_{in,2} + b_{1,2}\right)b_{8,2} - \left(G_{in,1} + b_{1,1}\right)b_{8,1} + b_{2,2}b_{9,2} - b_{2,1}b_{9,1} + b_{4,2}b_{10,2} - b_{4,1}b_{10,1}\end{array}\right\}$$

mass flux dynamics at the inlet of channel 1 (under parallel channel boundary conditions)

3.2.3 Steady-state and dynamic solutions

Firstly, steady-state conditions of the analysed system are obtained by solving the whole set of equations with time derivative terms set to zero. Steady-state solutions are then used as initial conditions for the integration of the equations, obtaining the time evolution of each computed state variable.

Input variable perturbations can be introduced both in terms of step variations and ramp variations.

The described dynamic model has been solved through the use of the MATLAB software SIMULINK® [23]. A suitable set of Matlab Functions has been defined to compute at each time step the dynamic coefficients listed in Table 5, based on the values of the state variables at the previous time step. Integrator Function Block has been finally used to integrate the whole set of non-linear ODEs – Eq.(60) –. Figure 15 shows the graphical interface of the developed model.

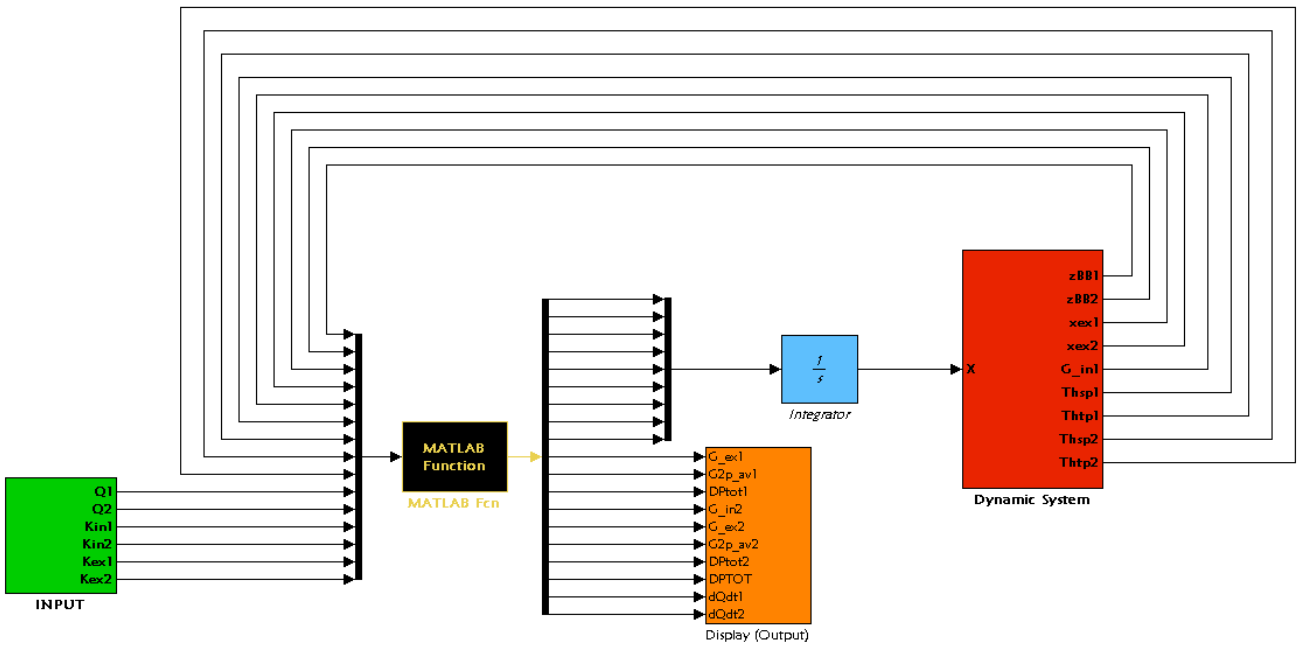

Figure 15 - SIMULINK® model scheme (two parallel channels configuration).

To excite the unstable modes of parallel channels oscillations, two procedures can be followed:

i) by performing a small perturbation in the exit quality between the two channels. For instance, within the initial conditions it can be imposed:

$$y_3(0) = x_{ex,0} + \Delta x_{ex}$$
$$y_4(0) = x_{ex,0} - \Delta x_{ex} \qquad (62)$$

ii) by increasing the input power in both the channels, step-by-step, up to the instability occurrence.

This second detection method has been mainly adopted, being the closest to what is done with the actual experimental procedure on the facility.

Theoretical predictions of the instability thresholds show that the simulated system passes from stable to unstable conditions according to the following process: damped oscillations – periodic oscillations – divergent oscillations. This concern is depicted in Figure 16, Figure 17 and Figure 18, where the behaviour of the mass flux at channel 1 inlet is displayed (directly from model graphical interface outputs) when a stable power level (Figure 16), threshold limit power (Figure 17), and an unstable power level (Figure 18) are respectively reached.

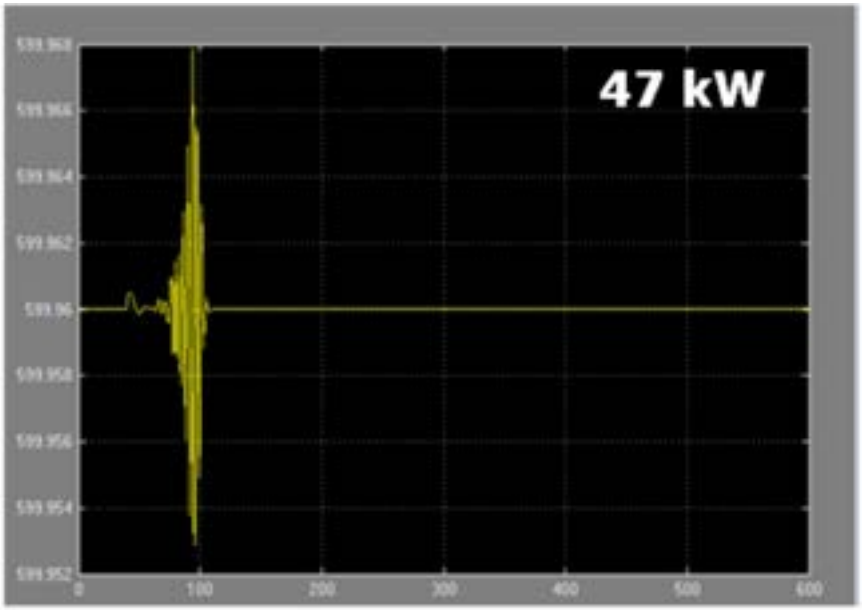

Figure 16 - Channel 1 inlet mass flux dynamic response to an increase of input thermal power (STABLE POWER LEVEL).
Simulated case: P = 20 bar; G_{in} = 600 kg/sm^2; T_{in} =208 °C; k_{in} = 100; k_{ex} = 0.

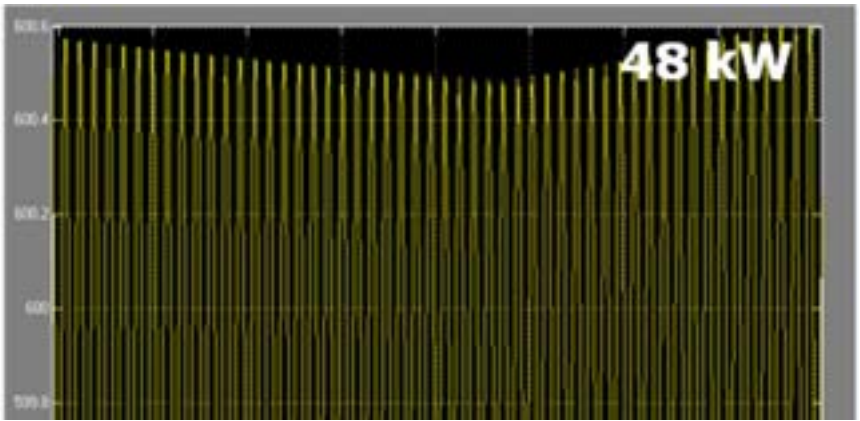

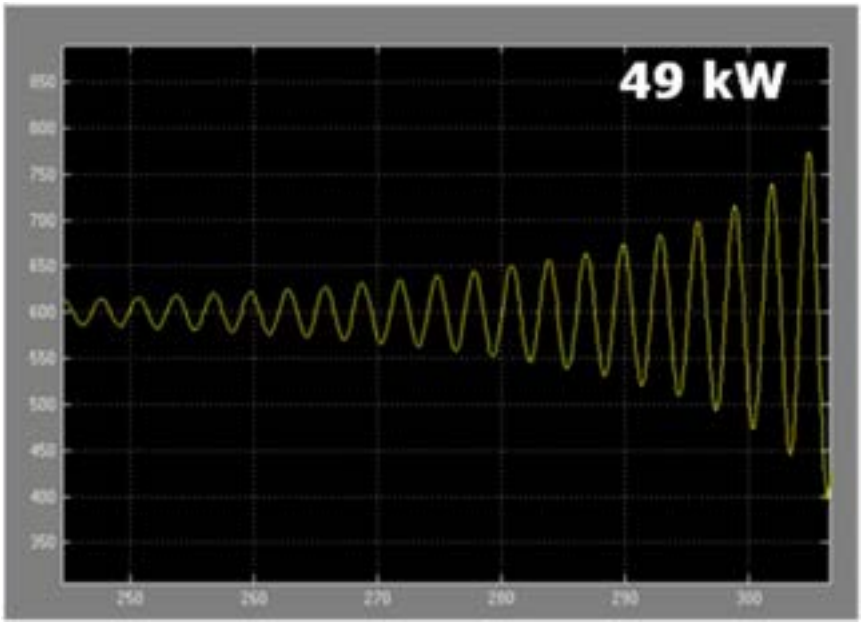

Figure 18 - Channel 1 inlet mass flux dynamic response to an increase of input thermal power (UNSTABLE POWER LEVEL).
Simulated case: P = 20 bar; G_{in} = 600 kg/sm^2; T_{in} =208 °C; k_{in} = 100; k_{ex} = 0.

3.3 Sensitivity of model predictions on two-phase friction factor multiplier

Specific empirical correlations are considered within momentum balance equation to duly represent flow behaviour, and in particular the frictional pressure drops inside a helically coiled tube. As concerns single-phase frictions, the friction factor *f* is evaluated with White correlation [24] for laminar regime, and Ito [25] and Ruffel [26] correlations for turbulent regime.

Model predictions demonstrated indeed to be extremely sensitive on the choice of the two-phase friction factor multiplier – Φ^2 in Eq.(22) –[4]. In order to quantify this sensitivity, and to understand which could be the most accurate correlation, the following calculational models have been implemented as separate functions within the developed code:

- Homogenous model (HEM-2), with inclusion of viscosity effects ("same Reynolds number dependence") [27];
- Martinelli-Nelson method, with Jones empirical correction factor [27][20];
- Chen correlation [28], which is indicated as the Chinese boiler hydrodynamic calculating method, and modified Chen correlation [24], with specific coefficient to account for helically coiled tubes;

[4] LIQUID ONLY approach is considered for two-phase friction multiplier, that is $\Phi_{lo}^2 = \frac{\Delta P_{tp}}{\Delta P_{lo}}$, where "lo" intends the liquid phase flowing alone with total flow rate.

- Friedel correlation [29], and modified Friedel correlation [30], recently tuned on the two-phase friction pressure drop data of Santini et al. [17] for helices (same helical-coiled test section used for the present experimental campaign, see Section 1.4).

For more computational details, consult the respective references. In the followings, the reader is just made aware of the three main approaches followed for the calculations.

3.3.1 HEM-2 model, with correction factor for viscosity effects

$$\Phi_{lo}^2 = \left[1 + x\left(\frac{v_{fg}}{v_f}\right)\right]\left[1 + x\left(\frac{\mu_{fg}}{\mu_f}\right)\right]^n \tag{63}$$

where *n* is equal to 0.25 for $\mathrm{Re} \le 2 \cdot 10^4$ (from Blasius correlation), and equal to 0.2 for $\mathrm{Re} > 2 \cdot 10^4$ (from McAdams correlation).

3.3.2 Chen correlation, modified by Guo for helical tubes

$$\Phi_{lo}^2 = \psi\psi_1\left[1 + x\left(\frac{\rho_f}{\rho_g} - 1\right)\right] \tag{64}$$

where ψ is a semi-theoretical coefficient:

$$\begin{aligned} \psi &= 1 + \frac{x(1-x)((1000/G)-1)(\rho_f/\rho_g)}{1 + x((\rho_f/\rho_g)-1)} && for\ G \le 1000 \\ \psi &= 1 + \frac{x(1-x)((1000/G)-1)(\rho_f/\rho_g)}{1 + (1-x)((\rho_f/\rho_g)-1)} && for\ G > 1000 \end{aligned} \tag{65}$$

ψ_1 is an empirical correction coefficient to exhibit the feature of helical coils, and is obtained from Guo's experimental data [24] of two different-sized coils:

$$\psi_1 = 142.2\left(\frac{p}{p_{cr}}\right)^{0.62}\left(\frac{D}{D_{coil}}\right)^{1.04} \tag{66}$$

3.3.3 Friedel correlation, modified for helical tubes

Modified Friedel correlation is introduced by Colorado et al. [30], optimizing the original Friedel correlation [29] basing on the experimental database of Santini et al. [17] on two-phase pressure drop measurements in helically coiled tubes. This correlation is of great interest for this work, because it is obtained from SIET experiences on the same coiled tube that is part of the new "parallel channels" test section (same length, pitch and diameter of the coil). The correlation has the following form:

$$\Phi_{lo}^2 = E + \frac{0.2058FH}{Fr^{-0.1266}We^{-0.1312}} \tag{67}$$

where:

$$E = (1-x)^2 + x^2 \frac{\rho_f f_{go}}{\rho_g f_{fo}} \tag{68}$$

$$F = x^{0.78}(1-x)^{0.224} \tag{69}$$

$$H = \left(\frac{\rho_f}{\rho_g}\right)^{0.91} \left(\frac{\mu_g}{\mu_f}\right)^{0.19} \left(1-\frac{\mu_g}{\mu_f}\right)^{0.7} \tag{70}$$

$$\rho_H = \frac{\rho_f \rho_g}{x\rho_f + (1-x)\rho_g} \quad \text{homogeneous density, as in Eq.(7)} \tag{71}$$

$$Fr = \frac{G^2}{gD\rho_H^2} \tag{72}$$

$$We = \frac{G^2 D}{\rho_H \sigma} \tag{73}$$

Instability threshold data, collected using the different models discussed for two-phase friction multiplier, have been clustered into stability maps. According to the theory introduced in Section 1.2, the stability maps on the Ishii and Zuber space (N_{sub} vs. N_{pch}) permit to easily identify stable and unstable regions.

The twin channel system preliminarily investigated with the RELAP5 code in Section 2.4 is considered. This is properly representative of the facility configuration tested at SIET labs. Geometrical data are those of Table 3. No exit loss coefficients (k_{ex}) are introduced, in accordance with the absence of valves downstream the test section tubes (see Figure 5). The destabilizing effect of the presence of a riser section (non-heated last 8 m) is well depicted in Figure 19, where the system stability is compared with a case without the unheated test section portion. The shift to the right of the threshold boundary by removing the riser widens in fact the stability region.

With reference to the full model of SIET facility (24 m heated portion and 8 m unheated portion), the different stability predictions given by the two-phase friction models above discussed are shown in Figure 20. Pretty different stability margins result according to the selected friction model. The system is most unstable (smallest stability region) considering Guo models, whereas, on the other hand, the utilization of modified Friedel equation highly increases the system stability. The order of increased system stability for the proposed models is: Guo – original Friedel – HEM-2 – modified Friedel.

It is worth noticing how the predictions of modified Friedel model (reasonably the closer one to the real frictional characteristics of SIET experimental facility) are remarkably more stable than all the other models. Finally, the boundary preliminarily predicted in the same conditions with the RELAP5 code is shown in Figure 20-b. The strong stability of the model built with RELAP5, as discussed in Section 2.4, is hereby confirmed.

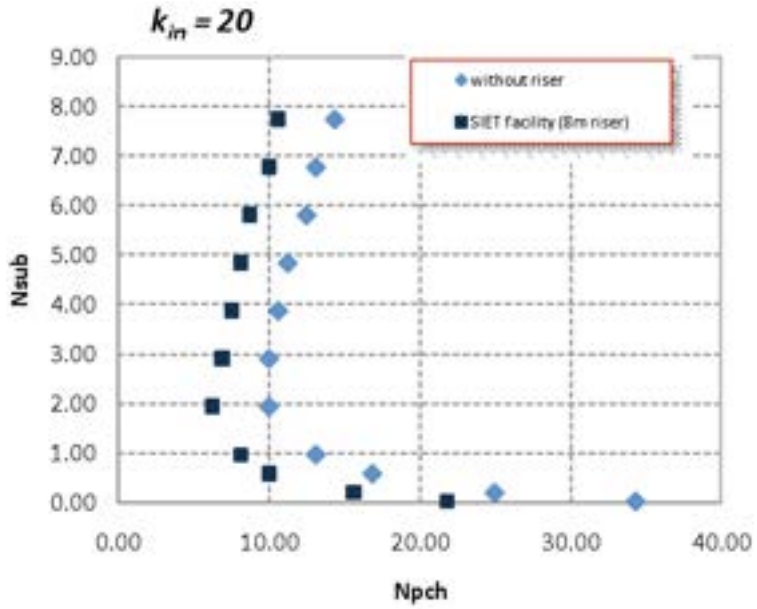

Figure 19 – Comparison between the stability maps theoretically obtained with and without system riser.
SELECTED MODEL: Martinelli with Jones-Dight correction factor.
$k_{in} = 20$; $k_{ex} = 0$.

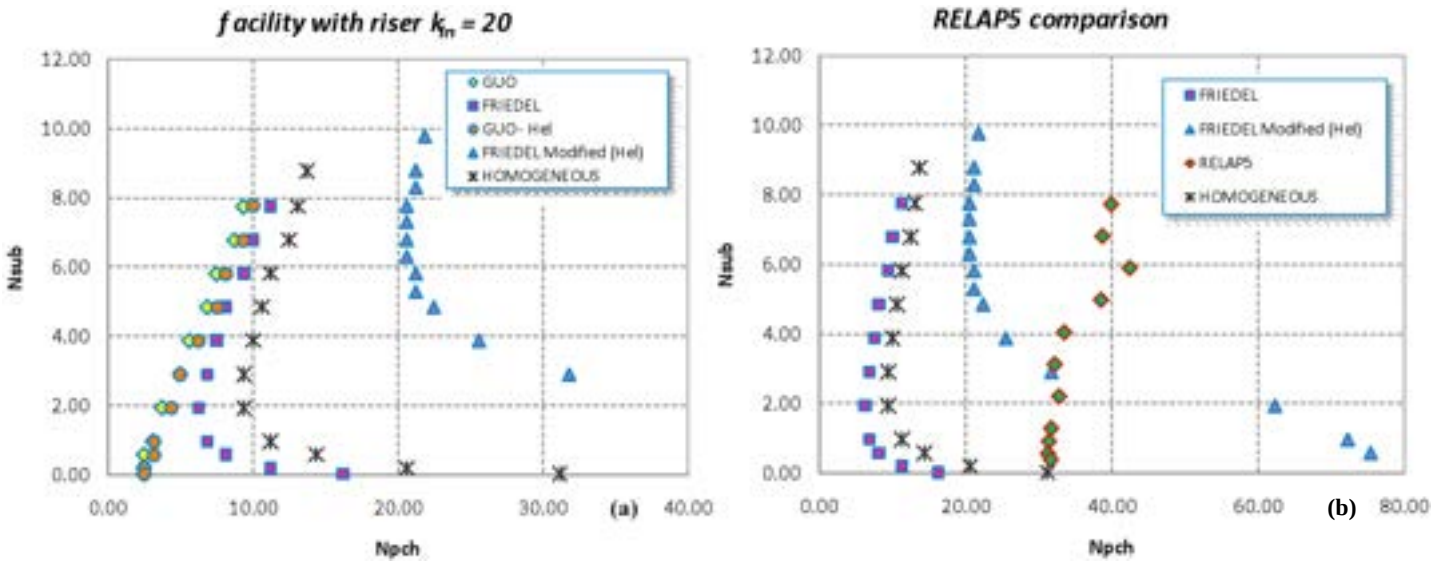

Figure 20 - Comparison between the stability maps theoretically obtained with different two-phase multiplier models.
$k_{in} = 20$; $k_{ex} = 0$.

3.4 Test matrix simulation

The described analytical model developed to theoretically predict DWO instability thresholds in parallel channels is used for the first simulations of the test matrix of the whole experimental campaign.

Due to the wide discrepancy between the various empirical models introduced (Section 3.3), the present pre-test analyses rely on the homogeneous two-phase multiplier model (HEM-2) [27], which is built on simple and more theoretical bases.

In accordance with what defined in Section 1.6, just two positions of tube inlet valves are taken into account:

- *Basically open valve configuration:* V1 and V2 valves are set in "-1 turn to valve closure position" (the respective inlet loss coefficients are estimated by means of the valve characterization as k_{in} = 45).
- *Partially closed valve configuration:* V1 and V2 valves are set in "-2/6 turn to valve closure position" (the respective inlet loss coefficients are estimated by means of the valve characterization as k_{in} = 100).

The results obtained with the first simulations on the test matrix are listed in the tables below. Possibility of thermal crisis occurrence is also accounted for, and a comparison of the instability limit power with first dryout power is established. First dryout power is calculated as the minimum value between CISE correlation for thermal crisis [31], and an empirical ad-hoc correlation developed by Santini [32] with dedicated experiences on the single helical-coiled tube facility.

- **Instability thresholds at P = 40 bar // G = 600 kg/sm^2**

  T_{sat} = 250.4 °C

k_{in}	*Pump mass flow [kg/h]*	*Inlet temperature [°C]*	*Subcooling degree [%]*	***Predicted limit power [kW]***	*First dryout power [kW]*
45	532.7	175	-20.1 %	**48**	135
45	532.7	195	-15.0 %	**42**	128
45	532.7	214	-10.0 %	**37**	122
45	532.7	223	-7.6 %	**36**	119
45	532.7	232	-5.1 %	**38**	116
45	532.7	243	-2.1 %	**58**	112
45	532.7	248	-0.7 %	**94**	110
100	532.7	175	-20.1 %	**62**	135
100	532.7	195	-15.0 %	**57**	128
100	532.7	214	-10.0 %	**55**	122
100	532.7	223	-7.6 %	**57**	119
100	532.7	232	-5.1 %	**66**	116
100	532.7	243	-2.1 %	**106**	112
100	532.7	248	-0.7 %	**stable**	110

- **Instability thresholds at P = 40 bar // G = 400 kg/sm^2**

  T_{sat} = 250.4 °C

k_{in}	*Pump mass flow [kg/h]*	*Inlet temperature [°C]*	*Subcooling degree [%]*	***Predicted limit power [kW]***	*First dryout power [kW]*
45	355.1	175	-20.1 %	**32**	87
45	355.1	195	-15.0 %	**28**	82
45	355.1	214	-10.0 %	**25**	78
45	355.1	223	-7.6 %	**24**	76
45	355.1	232	-5.1 %	**26**	74
45	355.1	243	-2.1 %	**38**	71
45	355.1	248	-0.7 %	**60**	70

- **Instability thresholds at P = 20 bar // G = 600 kg/sm^2**

  T_{sat} = 212.5 °C

k_{in}	*Pump mass flow [kg/h]*	*Inlet temperature [°C]*	*Subcooling degree [%]*	***Predicted limit power [kW]***	*First dryout power [kW]*
45	532.7	148	-15.1 %	**32**	145
45	532.7	170	-10.0 %	**25**	138
45	532.7	180	-7.7 %	**22**	135
45	532.7	191	-5.1 %	**19**	131
45	532.7	198	-3.5 %	**18**	129
45	532.7	204	-2.0 %	**20**	127
45	532.7	208	-1.1 %	**28**	126
45	532.7	210	-0.6 %	**37**	125
100	532.7	148	-15.1 %	**39**	145
100	532.7	170	-10.0 %	**32**	138
100	532.7	180	-7.7 %	**29**	135
100	532.7	191	-5.1 %	**27**	131
100	532.7	198	-3.5 %	**28**	129
100	532.7	204	-2.0 %	**34**	127
100	532.7	208	-1.1 %	**48**	126
100	532.7	210	-0.6 %	**63**	125

- **Instability thresholds at P = 80 bar // G = 600 kg/sm^2**

  T_{sat} = 295.1 °C

k_{in}	*Pump mass flow [kg/h]*	*Inlet temperature [°C]*	*Subcooling degree [%]*	***Predicted limit power [kW]***	*First dryout power [kW]*
45	532.7	157	-45.1 %	**95**	127
45	532.7	195	-33.6 %	**84**	115
45	532.7	238	-20.0 %	**75**	101
45	532.7	253	-15.1 %	**77**	95
45	532.7	268	-9.9 %	**88**	90
45	532.7	275	-7.5 %	**102** [5]	87
45	532.7	282	-4.9 %	**stable**	85

Instability data are clustered into stability maps in the Ishii-Zuber space (Figure 21 and Figure 22). It is apparent that closing the throttling valves at inlet increases the system stability. In both the reported graphs, stability boundaries obtained with partially close valve configuration (-2/6) are remarkably right-shifted if compared to open valve configuration case (-1).

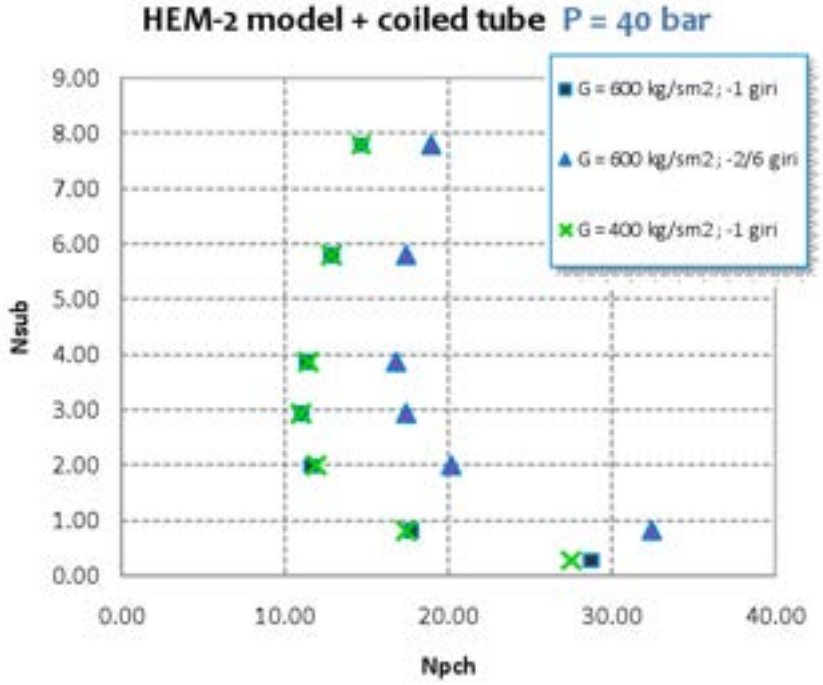

Figure 21 - Stability maps obtained with HEM-2 friction model at different mass fluxes and inlet valve positions.

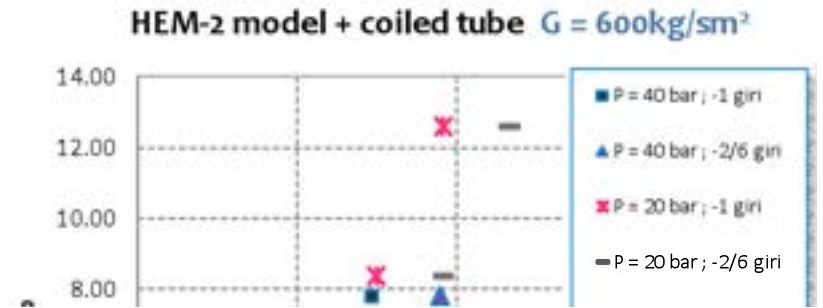

[5] The corresponding fore the flow oscillation threshold.

Moreover, the validity of such stability map is brilliantly confirmed, since the built stability boundaries depend just on tube inlet loss coefficient (valve k_{in}, as above), but are independent on the flow rate and on the pressure. The arguments of Section 1 find their corroborations in Figure 21, dealing with different mass fluxes at constant pressure level, and in Figure 22, dealing with different pressures at constant mass flow simulated.

Predictions of the period of oscillations at various inlet subcoolings are compared to the analytical calculations already discussed in Section 2.3. The ratio between the simulated oscillation period and the mixture transit time in the heated section (calculated according to Eq.(7)) is reported in Figure 23. Correlation to transit time in the riser is not considered, also due to the small values exhibited (on average 1-2 s).

According to literature results [1], the period of oscillations grows with the subcooling number, and is found to increase with a decrease of mass flow (the fluid is slower) and a decrease of pressure. The correlation with the calculated heated section transit time is such to be almost respected, being quite independent on the pressure and on inlet loss coefficient (valve position), but not on the mass flux. The ratio T/τ is in fact considerably smaller at low mass fluxes.

Moreover, if the results of Figure 23 are compared to the results obtained from RELAP5 in Figure 10, the ratio T/τ shows rather lower values, quite far from the twice ratio – Eq.(1) – deriving from the classical theory on density wave oscillations [1][2]. It is just mentioned that now a long test section (24 m of heated section against 3.66 m of RELAP5 analyses – Figure 10 –) is considered, and this could deeply affect the results.

Finally, the prediction of the oscillation period sounds quite strange at very low inlet subcooling conditions ($N_{sub} < 2$), where the simulated period drops to extremely low values (and so does the ratio T/τ). The oscillation period T, predicted for medium-high subcoolings in a range comprised between 10 and 40 s according to the pressure and mass flux investigated, drops to couple of seconds for x_{in} < 1-2%. Considered the long test section feature, a period of 2-3 s is quite inconsistent with the calculations of the mixture transit time, that should claim that the model could fail in a

proper representation of DWO instability phenomenon at very low inlet subcoolings. The strong hypotheses assumed during the model construction, above all the lumped approach which does not account for temperature propagation in the single-phase region (local temperature changes simultaneously at all the axial locations) could be a plausible explanation. Confrontation with the real behaviour of the simulated facility – coming from experimental tests execution (Section 4) – is mandatory to clarify this concern.

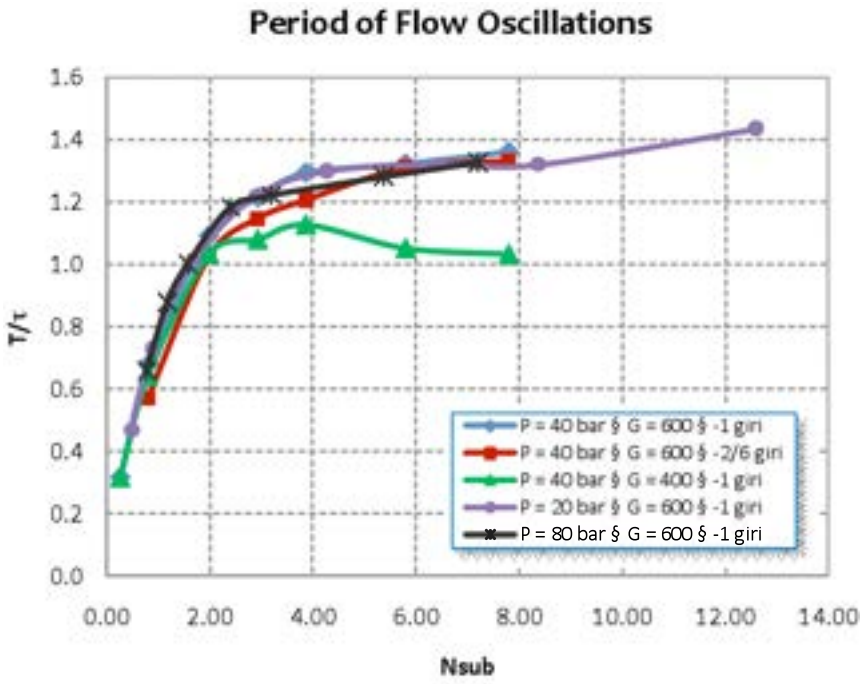

Figure 23 - Ratio between the period of oscillations and the calculated analytical transit time in the heated section, for various conditions simulated.

4 FIRST RESULTS OF THE EXPERIMENTAL CAMPAIGN

The experimental campaign at SIET labs started in the month of July 2010, thus the first data collected are already available and will be presented in this Section.

4.1 Valves characterization

As pointed out earlier in Section 1.6, the first activity carried out was the characterization of the valves, to analyse the different valve positions and calibrate the orifices with differential pressure transmitters, used as flow meters at the inlet of the two tubes.

Numerous tests were conducted with different valve positions, one tube at a time, starting from fully open till -1/6 turn to valve closure. All valve positions were tested in both cold-system condition (water temperature ≈ 30°C, mass flow rate 300 kg/h and 200 kg/h) and hot-system condition (water temperature ≈ 200-210°C, mass flow rate 300 kg/h, 200 kg/h, 150 kg/h and 80 kg/h, no heating power to the test section). Data acquisition was focused on the pressure drops across the calibrated orifices, valves and the system valve+orifice. The data permitted to draw calibration curves relating a pressure loss coefficient *k* to every single valve position. It is reminded that for a fixed value of water density, the pressure drop across the valve is function of the mass flow rate through the coefficient *k*:

$$\Delta P = \frac{1}{2} k \frac{G^2}{\rho_{in}} \tag{74}$$

Figure 24 shows the calibration curves for the two valve positions selected in Section 1.6 as reference for the experimental campaign (k_1= -1 turn, slight pressure drop, k_2=-2/6 turn, noticeable pressure drop).

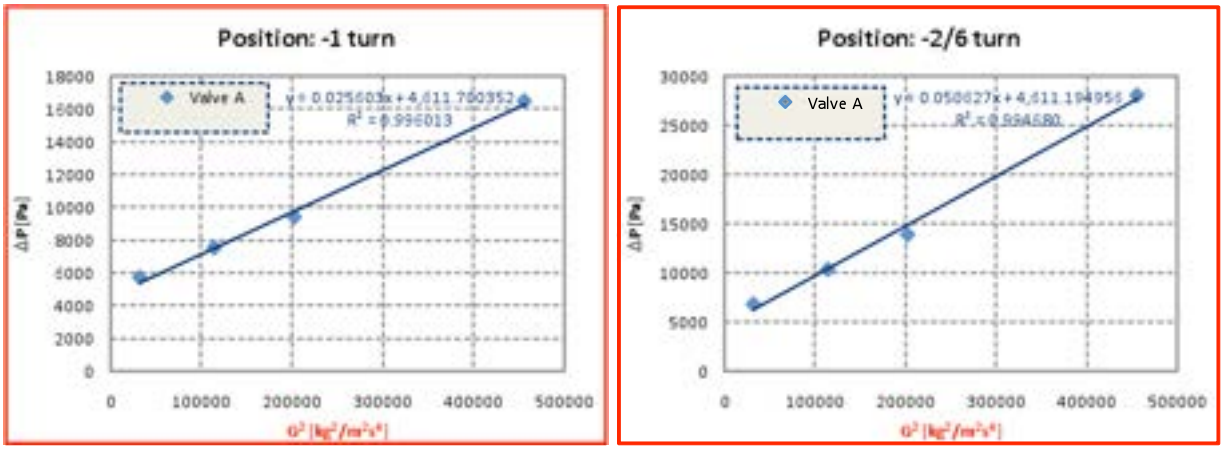

Figure 24 - Calibration curves for valve A in two different positions (k_1=-1 turn to valve closure and k_2=-2/6 turn to valve closure).

4.2 Experimental results

First experiments were conducted with the following system parameters: system pressure 40 bar (medium value, see Section 1.6), single channel mass flux 600 kg/m^{2}s (not so much lower than IRIS steam generator nominal value), valve

position -1 turn to valve closure (slight pressure drop introduced, basically open valve configuration). A preliminary stability map was obtained exploring different inlet subcoolings and following the procedure illustrated in Section 1.5 to reach the power level at which the system becomes unstable. A total of 8 different inlet temperatures were investigated. Moreover, two more points were found decreasing the mass flux to 400 kg/m^{2}s. All the experimental points are resumed in Table 6, in which mass flux and power supplied are referred to a single channel.

Table 6 - First set of experimental data.

P [bar]	G [kg/m^{2}s]	k_1	k_2	T_{in} [°C]	x_{in} [%]	N_{sub}	Q_T [kW]	N_{pch}
40.83	600.9	-1 turn	-1 turn	155.3	-25.5%	9.66	94.78	28.34
40.42	600.3	-1 turn	-1 turn	175.1	-20.3%	7.77	88.42	26.73
40.38	601.6	-1 turn	-1 turn	195.2	-15.1%	5.78	84.65	25.56
40.93	600.3	-1 turn	-1 turn	194.7	-15.5%	5.84	85.10	25.41
39.95	603.4	-1 turn	-1 turn	213.0	-10.2%	3.97	87.33	26.57
39.97	601.5	-1 turn	-1 turn	215.5	-9.55%	3.71	89.52	27.31
40.78	602.7	-1 turn	-1 turn	222.8	-8.0%	3.02	79.60	23.76
40.42	604.0	-1 turn	-1 turn	231.2	-5.5%	2.12	72.29	21.72
40.65	602.6	-1 turn	-1 turn	238.2	-3.7%	1.40	62.18	18.62
40.59	399.4	-1 turn	-1 turn	223.3	-7.76%	2.96	54.91	24.84
41.05	396.9	-1 turn	-1 turn	233.3	-5.23%	1.97	49.76	22.41

The preliminary stability map (only two points were collected at 400 kg/m^{2}s) is shown in Figure 25. The system is found to be more stable if compared with analytical model predictions (Figure 21 and Figure 22). However, the stable region results smaller if compared with RELAP5 predictions (Figure 14). The numerical code seems to approximate better the shape of the experimental stability boundary (although the map shown in Section 2.4 was calculated with slightly different system parameters).

The experimental curve shape deviates from classical theory of DWOs, especially at low subcoolings. As a matter of fact, the subcooling stabilizing effect at low inlet temperatures is confirmed, whereas, at higher inlet temperatures, the subcooling destabilizing effect, predicted from theory, is not apparent. As can be seen from Figure 25, the stability curve is near a straight line and the subcooling stabilizing effect becomes higher at low subcoolings. At present, a clear explanation has not been developed yet. However, it must be remarked that just one configuration of the system has been tested, and more experimental points will be collected in the near future to explain more clearly and to better understand the whole phenomenon. In particular, a deeper insight is needed concerning the effect of helically shaped tubes and long test section feature on the onset of instability.

Figure 26 exhibits the same trend. Limit power (for system stability) is shown as a function of the inlet subcooling. Limit power value reduces significantly decreasing the subcooling from -10% to under -5%. Even if only two points were collected at 400 kg/m^{2}s, they seem to confirm the highlighted behaviour.

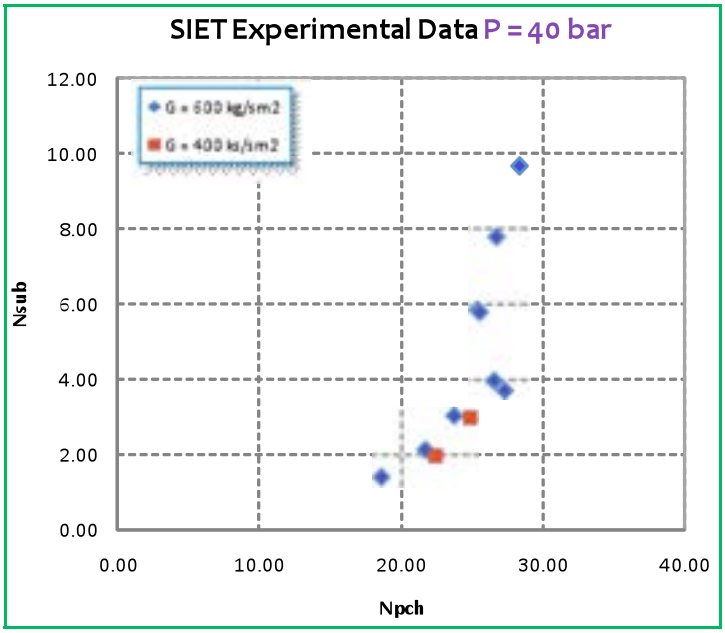

Figure 25 - Stability maps obtained from experimental data.

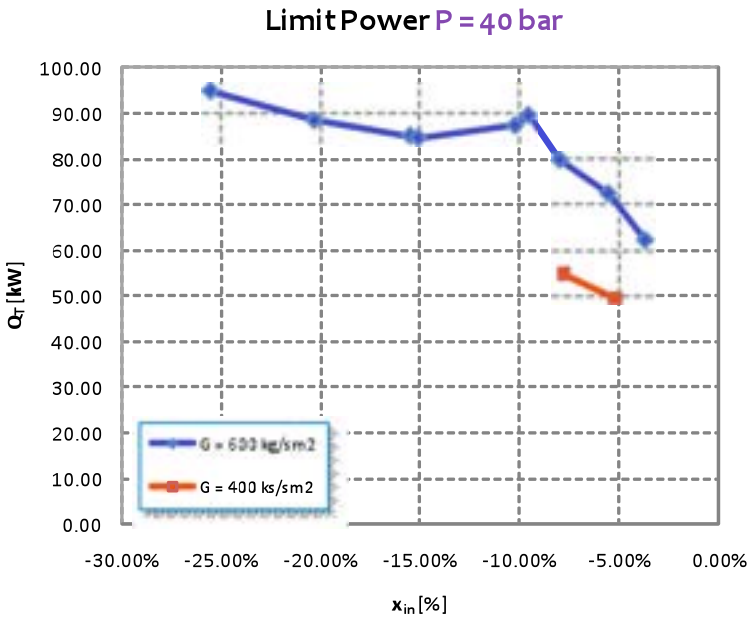

Figure 26 - Limit power for system stability as a function of the inlet subcooling.

The unstable conditions were reached experimentally with electrical power steps of 3-5 kW (1.5 - 2.5 kW per tube) at a time, separated by a sufficient time to allow the system reaching steady-state. The procedure permitted numerous data acquisitions in different system conditions. Data were collected in steady-state, during transient in stable conditions, incipient instability, transient from stable to unstable operation and also recording fully-developed instability. In certain conditions, as far as five minutes of fully-developed instability data were collected recording the distinctive features of DWOs (without damages to test section tubes).

Figure 27 shows pressure drop oscillations across calibrated orifices of both channels. Data refer to fully-developed instability at 100 kW of electrical power and 214 °C of inlet temperature. In agreement with literature, the oscillations in the two channels occur in counter-phase.

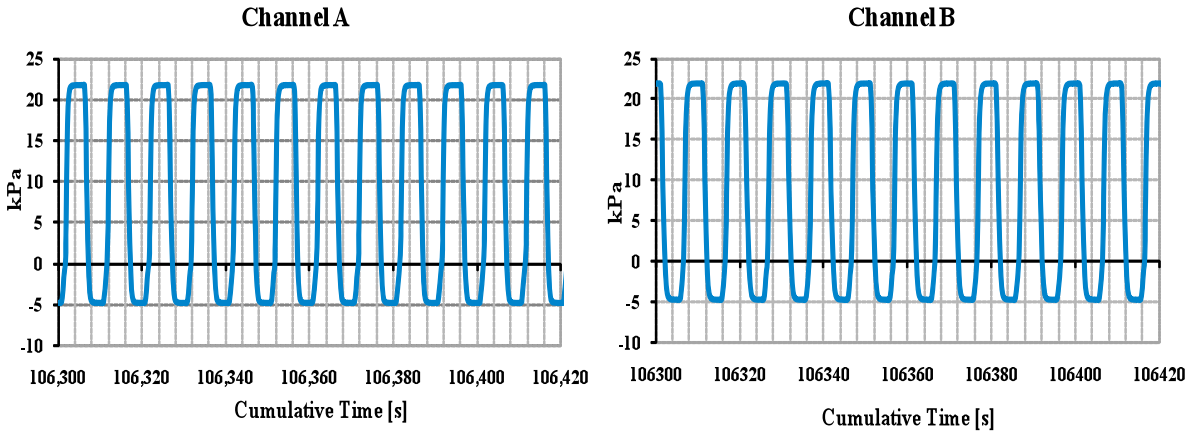

Figure 27 - Pressure drop oscillations across the calibrated orifices of both channels in fully-developed instability conditions. *SYSTEM PARAMETERS*: electrical power per channel 100 kW, inlet temperature 214 °C, mass flux 600 kg/m^{2}s, system pressure 40 bar.

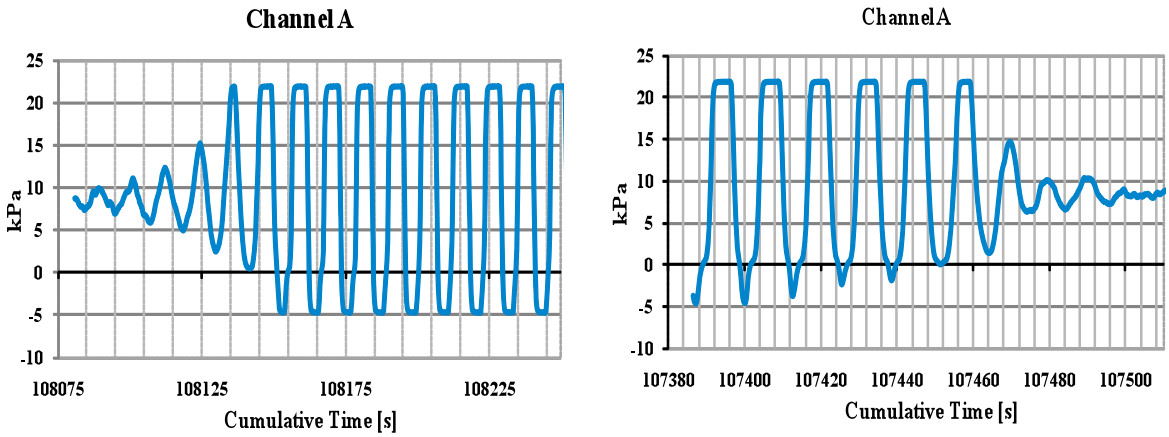

Figure 28 - Pressure drop across channel A calibrated orifice, by increasing and decreasing the electrical power near 100 kW. *SYSTEM PARAMETERS*: inlet temperature 214 °C, mass flux 600 kg/m^{2}s, system pressure 40 bar.

Transition from stable to unstable conditions – increasing electrical power – and oscillation damping – decreasing electrical power – were registered as well (Figure 28). Data are related to pressure drops on the calibrated orifice of channel A.

Counter-phase oscillation of single-phase and two-phase pressure drops within each channel is known to be one of the triggering events leading to the appearance of DWOs [1]. Data collected during fully-developed oscillations permitted to verify the previous condition comparing the pressure drops recorded by different pressure taps placed on channel A. Figure 29 shows the pressure drops between taps 2 and 3 (single-phase region) and taps 5 and 6 (two-phase region). The counter-phase oscillation is clearly visible. Moreover, total system pressure oscillates with a frequency that is double when compared with the flow rate in each channel (Figure 30). Reported graphs represent both pressure drop across channel A calibrated orifice (representative of flow rate in channel A) and absolute system pressure measured at the exit (outlet header). Also "thermal oscillations", featured by large wall temperature oscillations, are induced by DWOs (as described by Kakaç and Bon [2]). Wall temperatures recorded during a fully-developed instability are presented in Figure 31. Wall thermocouples are attached at the same channel height in four circumferential positions (channel A).

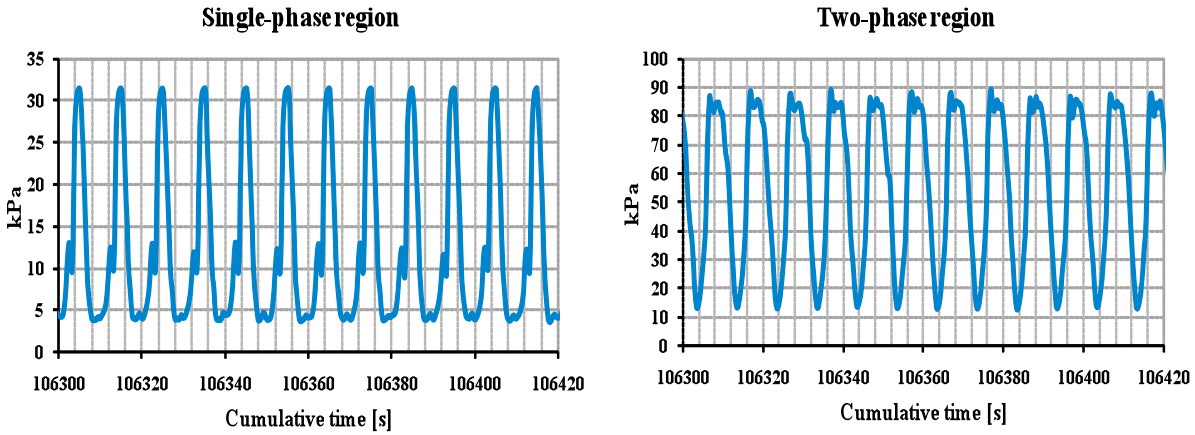

Figure 29 - Counter-phase pressure drop oscillations in single-phase and two-phase region during fully-developed oscillation. *SYSTEM PARAMETERS*: electrical power per channel 100 kW, inlet temperature 214 °C, mass flux 600 kg/m^{2}s, system pressure 40 bar.

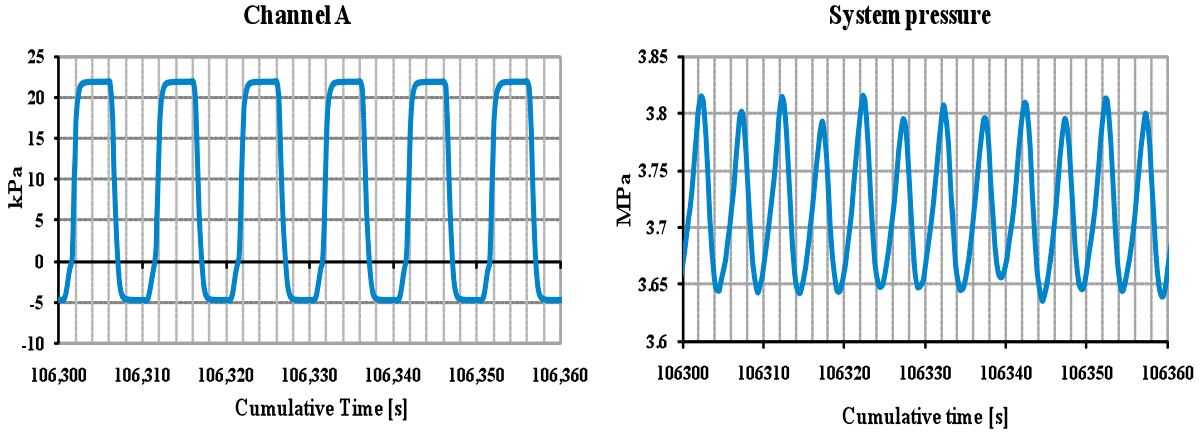

Figure 30 - Channel A calibrated orifice pressure drop oscillation compared with exit system pressure oscillation. *SYSTEM PARAMETERS*: electrical power per channel 100 kW, inlet temperature 214 °C, mass flux 600 kg/m^{2}s, system pressure 40 bar.

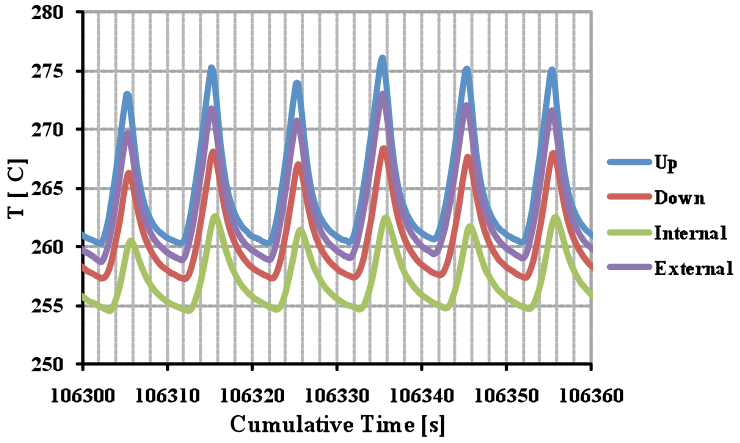

Figure 31 - Wall temperature oscillations. *SYSTEM PARAMETERS*: electrical power per channel 100 kW, inlet temperature 214 °C, mass flux 600 kg/m^{2}s, system pressure 40 bar.

The period of oscillations is now discussed. During DWOs, since a complete oscillating cycle consists in the passage of two perturbations through the channel (classical theory explanation [1]), the period of oscillations should be in the range of twice the mixture transit time in the heated section. In addition, accordingly to a different description raised in the recent years [8][9], at high inlet subcoolings the period of the oscillations may be considerably longer than twice the fluid transit time.

Hence, the period of oscillations is expected to become smaller together with the transit time when decreasing the inlet subcooling. The experimental data at 600 kg/m^{2}s of mass flux exhibit however an opposite trend, as the period of oscillations increases with lower inlet subcoolings (Figure 32). Such particular behaviour could be somehow consistent with the stability map presented in Figure 25, in which the stabilizing effect at low subcoolings does not appear. The two effects seem to be connected and triggered by the same phenomenon. The two data at 400 kg/m^{2}s of mass flux are not sufficient to gain additional information on the subject. Also the ratio between period of oscillations (T) and mixture transit time (τ) grows reducing the inlet subcooling, in contrast with classical DWOs theory as well (Figure 33).

Consistently with the theoretical results obtained with the analytical model in Section 3.4 (see Figure 23), the period of oscillation is higher at low mass fluxes (fluid flow is slower), and the ratio T/τ is basically lower than 2 (as should be from theory). Conversely, the lower values (much less than 2) are obtained at the high inlet subcoolings (opposite trend with respect to the model). Figure 33 shows also that the described behaviour is not due to the riser section, which introduces only a negligible deviation on the period of oscillations-transit time ratio.

In conclusion, two are the issues still far from a complete understanding, to which the next experimental tests from September 2010 and the related research activities in the near future will be addressed.

(i) *To deeply investigate the behaviour of the parallel channel system at low inlet subcoolings.* The apparent destabilizing effect of a reduction of inlet subcooling (up to saturation) is anyhow confirmed by a recent work due to Guo Yun et al. [33] about an experimental study on two-phase flow instability in a parallel twin-channel system (with straight tubes).

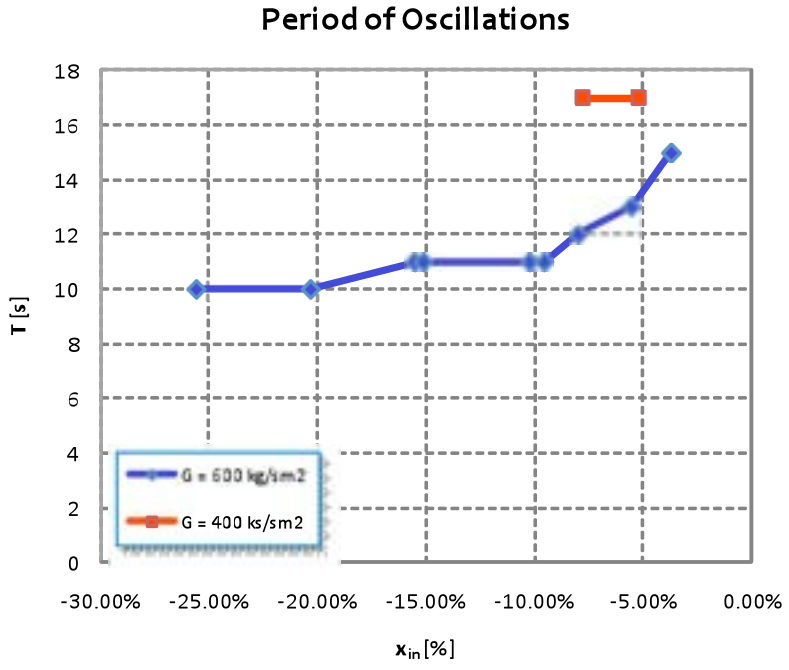

Figure 32 - Period of oscillations characterizing experimental instability points.

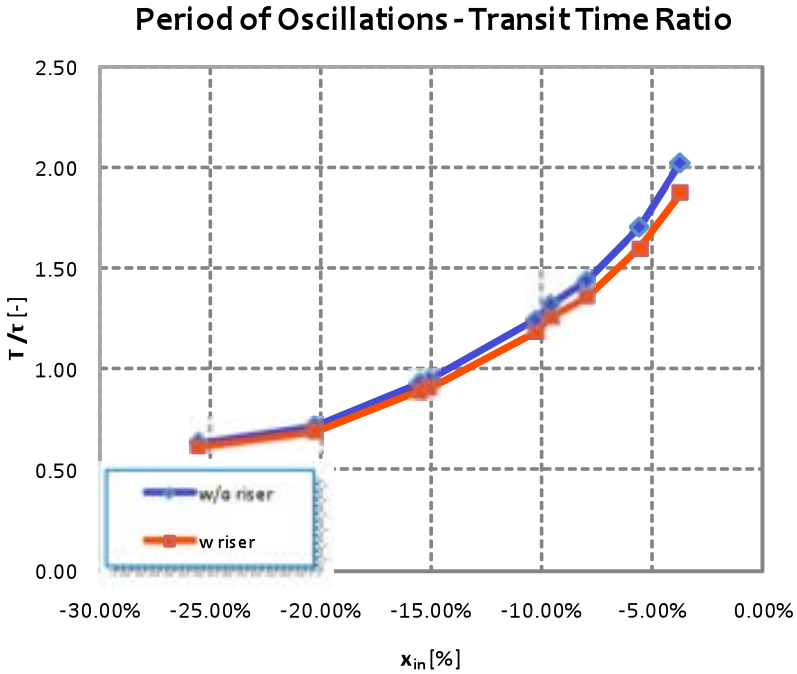

Figure 33 - Ratio between period of oscillations and mixture transit time at 600 kg/m^{2}s.

To this concern, it is just noticed that collecting experimental threshold data at low inlet subcooling conditions is not easy task. Under fully-developed oscillation conditions, all the system exhibits a periodic behaviour (mass flow in each channel, pressure, wall temperatures, fluid temperatures), such that also the temperature at the inlet of each tube is characterized by large amplitude oscillations. When increasing the inlet temperature via the pre-heater (testing low inlet subcooling conditions), these large oscillations lead the fluid at inlet instantaneously to saturation conditions, which could promote directly the evaporation process when heat is transferred from the wall. The hypothetical presence of steam at channel inlet is ascribed as a destabilizing effect on the system behaviour.

(ii) *To interpret the period of oscillations with respect to classical theory and heated section transit time.* To this aim, both the long test section feature (in comparison with literature works), and the helical coil shape (with the centrifugal field that interacts with the fluid flow along the channels [6]) should be properly considered.

[6] For instance, the influence of centrifugal field on the recorded DWOs is made apparent if considering the wall temperature oscillations shown in Figure 31. The instability amplitude (by means of its effect on tube wall) is in fact more marked in the UP and EXTERNAL circumferential positions.

REFERENCES

[1] G. Yadigaroglu, Two-Phase Flow Instabilities and Propagation Phenomena, In: J. M. Delhaye, M. Giot, M. L. Riethmuller, (Ed.), Thermohydraulics of two-phase systems for industrial design and nuclear engineering, Hemisphere Publishing Corporation, Washington, pp. 353-396, 1981

[2] S. Kakac, B. Bon, A Review of two-phase flow dynamic instabilities in tube boiling systems, *International Journal of Heat and Mass Transfer* 51, pp. 399-433, 2008.

[3] G. Yadigaroglu, A.E. Bergles, Fundamental and Higher-Mode Density Wave Oscillations in Two-Phase Flow, *Journal of Heat Transfer – Transactions of the ASME*, vol. 94, pp. 189-195, 1972.

[4] R.T. Lahey, Jr., E.J. Moody, The thermal-hydraulics of a boiling water nuclear reactor, American Nuclear Society, USA, 1977.

[5] N. Zuber, F.W. Staub, The Propagation and the Wave Form of the Vapor Volumetric Concentration in Boiling, Forced Convection System under Oscillatory Conditions, *International Journal of Heat and Mass Transfer*, vol. 9, pp. 871-895, 1966.

[6] N. Zuber, F.W. Staub, An Analytic Investigation of the Transient Response of the Volumetric Concentration in a Boiling Forced-Flow System, *Nuclear Science and Engineering*, vol. 30, pp. 268-278, 1967.

[7] W. Ambrosini, P. Di Marco, J.C. Ferreri, Linear and Nonlinear Analysis of Density Wave Instability Phenomena, *International Journal of Heat and Technology*, vol. 18, no. 1, pp. 27-36, 2000.

[8] M.Z. Podowski, Instabilities in Boiling Systems, In: Proceedings of Third International Topical Meeting on Nuclear Plant Thermal Hydraulics and Operations, Seoul, Korea, November 1988, pp. A1-88-A1-98, 1988.

[9] Rizwan-Uddin, Physics of Density Wave Oscillations, In: Proceedings of International Conference on 'New Trends in Nuclear System Thermohydraulics', Pisa, Italy, 30 May - 2 June, 1994.

[10] M. Ishii, N. Zuber, Thermally Induced Flow Instabilities in Two-Phase Mixtures, In: Proceedings of 4th International Heat Transfer Conference, Paris, France, August 1970, vol. 5, paper B5.11, 1970.

[11] Guo Yun, S.Z. Qiu, G.H. Su, D.N. Jia, Theoretical investigations on two-phase flow instability in parallel multichannel system, *Annals of Nuclear Energy*, vol. 35, pp. 665-676, 2008.

[12] Y.J. Zhang, G.H. Su, X.B. Yang, S.Z. Qiu, Theoretical research on two-phase flow instability in parallel channels, *Nuclear Engineering and Design*, vol. 239, pp. 1294-1303, 2009.

[13] G. Yadigaroglu, A.E. Bergles, An Experimental and Theoretical Study of Density-Wave Oscillations in Two-Phase Flow, MIT Tech. Rep., DSR 74629-3 (HTL 74629-67), 1969.

[14] D.D.B. Van Bragt, T.H.J.J. Van Der Hagen, Stability of natural circulation boiling water reactors: Part I – Description stability model and theoretical analysis in terms of dimensionless groups, *Nuclear Technology*, vol. 121, pp. 40-51, 1998.

[15] M. Ishii, Study of Flow Instabilities in Two-Phase Mixtures, Argonne National Laboratory Tech. Rep., ANL-76-23, 1976.

[16] G. Masini, G. Possa, F.A. Tacconi, Flow instability thresholds in parallel heated channels, *Energia Nucleare*, vol. 15, no. 12, pp. 777-786, 1968.

[17] L. Santini, A. Cioncolini, C. Lombardi, M. Ricotti, Two phase pressure drops in a helically coiled steam generator, *International Journal of Heat and Mass Transfer* 51, pp. 4926-4939, 2008.

[18] L. Santini, D. Papini, M.E. Ricotti, Experimental Characterization of a Passive Emergency Heat Removal System for a GenIII+ Reactor, *Science and Technology of Nuclear Installations* Volume 2010, Article ID 864709, 12 pages, doi:10.1155/2010/864709, 2010

[19] W. Ambrosini, J. C. Ferreri, Analysis of Basic Phenomena in Boiling Channel Instabilities with Different Flow Models and Numerical Schemes", In: Proc. 14th International Conference on Nuclear Engineering (ICONE 14), Miami, Florida, USA, July 17-20, 2006.

[20] J.L. Muñoz-Cobo, M.Z. Podowski, S. Chiva, Parallel channel instabilities in boiling water reactor systems: boundary conditions for out of phase oscillations, *Annals of Nuclear Energy*, vol. 29, pp. 1891-1917, 2002.

[21] G.B. Wallis, One dimensional two-phase flow, McGraw-Hill, 1969.

[22] F.P. Incropera, D.P. Dewitt, T.L. Bergman, A.S. Lavine, Fundamentals of heat and mass transfer, John Wiley & Sons, USA, 2007.

[23] SIMULINK® software, The MathWorks, Inc., 2005.

[24] L. Guo, Z. Feng, X. Chen, An experimental investigation of the frictional pressure drop of steam-water two-phase flow in helical coils, *International Journal of Heat and Mass Transfer* 44, pp. 2601-2610, 2001.

[25] H. Ito, Friction factors for turbulent flow in curved pipes, *Journal of Basic Engineering*, pp.123-134, 1959.

[26] A.E. Ruffel, The application of heat transfer and pressure drop data to the design of helical coil once-through boilers, Symposium Multi-Phase Flow Systems, University of Strathclyde, *Institution of Chemical Engineers Symposium Series* 38, Paper 15, 1974.

[27] N.E. Todreas, M.S. Kazimi, Nuclear Systems I: Thermal-hydraulic Fundamentals, Taylor & Francis, 1993.

[28] L. Chen, Steam-water two-phase flow frictional pressure drop in straight tubes, In: X. Chen (Ed.), Selected Papers of Multiphase Flow and Heat Transfer, Paper 7, Xi'an Jiaotong University Press, 1982, pp. 7.1-7.6.

[29] L. Friedel, Improved friction pressure drop correlation for horizontal and vertical two-phase pipe flow, European Two-Phase Flow Group Meeting, Ispra, Italy, Paper E2, 1979.

[30] D. Colorado, D. Papini, J.A. Hernández, M.E. Ricotti, Development and experimental validation of a computational model for a helically coiled steam generator, *International Journal of Thermal Sciences*, Under Review.

[31] C. Lombardi, Impianti Nucleari, Sesta Edizione, Edizioni CUSL, 2004.

[32] L. Santini, Thermalhydraulic issues of IRIS nuclear reactor helically coiled steam generator and emergency heat removal system, PhD Thesis, Dipartimento di Ingegneria Nucleare, Ciclo XX, Politecnico di Milano, Milan, June 2008.

[33] Guo Yun, Huang Jun, Xia Genglei, Zeng Heyi, Experimental investigation on two-phase flow instability in a parallel twin-channel system, *Annals of Nuclear Energy* 37, pp. 1281-1289, 2010.